Interaction of Coated Mild Steel and Cooling Systems, A DFT Approach

Fernandes, Rikitha S.
Department of Chemistry, Bits Pilani Hyderabad, Hyderabad, INDIA

Salmataj, Taj
Department of Biotechnology, Manipal Institute of Technology, Manipal Academy of Higher Education (MAHE), Manipal, INDIA

Pushpanjali*[*+], Bhat
Department of Chemistry, Manipal Institute of Technology, Manipal Academy of Higher Education (MAHE), Manipal, INDIA

ABSTRACT: *The present work describes the corrosion inhibition of one of the widely used alloys in the industrial process, i.e., Mild Steel in Fresh water and demineralized water using acrylic polymer coating, Acrylic/8% $Zn_3(PO_4)_2$ coatings, and Acrylic/8% $Zn_3(PO_4)_2$/ 5mM AgNPs coating. The efficiency of coating on mild steel in fresh water and demineralized water was studied using suitable gravimetric and electrochemical techniques and the surface texture of mild steel after coating was studied by Scanning Electron Microscope. The electrochemical study reveals that the coating efficiency was found to decrease with an increase in temperature and Acrylic/8% $Zn_3(PO_4)_2$/5mM AgNPs exhibited the highest inhibition efficiency of 94% and 95% in fresh water and demineralized water respectively at 303K. The excellent corrosion coating performance is attributed to the physisorption process of adsorption of the coatings on the metal surface which in turn followed the Langmuir adsorption isotherm. The results obtained by both Tafel polarization and electrochemical impedance spectroscopy methods were in good agreement with each other. The density functional theory in the study of acrylic coating also supported the obtained experimental results. To sum up, the acrylic coating with and without 8% $Zn_3(PO_4)_2$/ 5mM AgNPs is an efficient corrosion coating material.*

KEYWORDS: *Acrylic, AgNPs, Zinc phosphate, Cooling water system, Mild steel.*

INTRODUCTION

We live in a metal-based world, where we make use of metals in our day-to-day lives for various purposes. Metals are used in various industries such as the paper and pulp industry, chemical and oil industries, power generation, and underground structures [1]. Mild steel, one of the most significant iron alloys, is utilized extensively across a wide range of sectors due to its superior mechanical properties, increased tensile strength, weldability, and cost-

* *To whom correspondence should be addressed.*
+E-mail: pushpa.bhat@manipal.edu
1021-9986/2023/11/3737-3763 27/$/7.07

effectiveness [2]. It has the inherent tendency to undergo tarnishing or deterioration due to the environment to which it is exposed by the process of Corrosion. It degrades the useful properties of metals/alloys including strength, appearance, and permeability to gases and liquids. Corrosion mitigation techniques have been developed, but coating appears to be the most effective strategy for protecting both metallic and non-metallic surfaces. This is because coating creates a physical barrier between the metal and the corrosive environment, delaying corrosion while also serving other purposes such as decontamination, easier cleaning, safety, and improved working conditions.

In cooling systems, mild steel is often employed (in heat exchanger tubings, transfer lines, baffles, and heat exchanger shells). It is common practice to employ cooling liquid systems to remove heat from industrial operational operations. Water is also frequently used as a coolant due to its superior heat transfer capabilities [3]. abundance, eco-friendly property, and easy handling. However, the operability and durability of steel are reduced due to malfunction caused by the presence of various chloride, sulfate, and other ions in the coolant and other factors such as temperature, pH, chloride content, hardness of the coolant that accelerates the corrosion process. Therefore, cooling water systems' design and operating problems have gained significant attention. In this regard, a wide variety of organic coatings with strong surface adherence and chemical inertness, like acrylic and epoxy coatings, have been used and are effective at reducing corrosion [4-6]. However, they have downsides, such as a deterioration in anti-corrosive effectiveness over time [7] as a result of ions' and molecules' permeability through the coating [7,8]. In addition to this, the use of phosphate coatings is one such widely accepted technique [9-11] for the surface treatment of various ferrous and non-ferrous alloys, but owing to its porosity, there can be a decrease in the anti-corrosion performance [12]. Since nanoparticles have unique features and could enhance the coating qualities, these limitations could be resolved by adding them to the coating structure [13–17]. It would act as a filler and improve the coating's [11,13] adherence to the metal, decreasing corrosion.

One such example is the nano SiO_2 incorporated nano zinc phosphate coatings, developed by *Tamilselvi et al.*, on mild steel for acquiring better corrosion protection. The findings showed that the presence of nanoscale SiO_2 in the phosphating solution altered the initial potential of the interface between the phosphating solution and the mild steel substrate decreased the activation energy of the phosphating process, increased the number of nucleation sites, and produced zinc phosphate coatings with higher coating weights, greater surface coverage, and improved corrosion resistance [13]. *Osama et al*. synthesized the hydrophobic nanocomposite coating ZnO with polystyrene and explored it for mild steel corrosion protection in NaCl (3.5%) solution with different percentages of ZnO. The EIS results highlighted a significant increase in the charge transfer resistance in the presence of PS/ZnO-5 [14]. *Milad et al*., studied hydrophobic polypropylene coating on mild steel to decrease the movement of corrosive agents in the presence and absence of additives of graphene oxide and grafted maleic anhydride. The results highlight that the addition of grafted maleic anhydride and graphene oxide to polypropylene increased the compactness, corrosion resistance, and surface smoothness [15]. *Edouk et al*. synthesized zirconia-modified acrylic nanocomposites. The inorganic/organic hybrid resin coating was applied on steel to prevent its corrosion in a 3.5 wt% NaCl solution. As a result of the presence of zirconia nanoparticles in the coating, which prevented ions and other molecules from penetrating it and slowed the corrosion of steel, it was determined that the zirconia-modified acrylic coating exhibited significant resistance against corrosion of steel in NaCl solution [19]. In addition, it was determined how many zirconia nanofillers were needed to create zirconia-modified acrylic nanocomposites with effective barrier characteristics.

Denture coatings still take less time to gel and cure than epoxy coatings, but the work done by using denture acrylic coating on mild steel is highly limited. In this study, we evaluated the anti-corrosion performance of acrylic polymer, acrylic + 8% Zinc phosphate coating, and 5mM nano-silver doped Acrylic+8% Zinc phosphate coating on mild steel in fresh water and Demineralized water (DM water) due to the limited corrosion studies on mild steel in fresh or demineralized water (for cooling systems) and the use of polymer coating with suitable filler material and nanocomposite polymer for corrosion studies.

Density Functional Theory (DFT) was used to conduct a theoretical analysis of acrylic coating's effectiveness in preventing corrosion. Calculated values include the highest occupied molecular orbital energy (E_{HOMO}), the lowest unoccupied molecular orbital energy (E_{LUMO}),

Table 1: Elemental composition of EN8 carbon steel

Element	C	Si	p	Mn	S	Fe
Composition (weight %)	0.0036	0.02	0.025	0.54	0.05	balance

the energy gap between E_{HOMO} and E_{LUMO} ($E = E_{HOMO} - E_{LUMO}$), dipole moment (D), electron affinity (A), ionization potential (I), the absolute electronegativity (χ), absolute hardness (η), and softness (σ), the Mulliken charges, and the fraction of electrons (ΔN) transfer from acrylic coating to iron have been calculated.

EXPERIMENTAL SECTION

Materials

The EN8 carbon steel used for the corrosion study has the composition given in Table 1.

Preparation of the material

For the weight-loss method, metal coupons with a diameter of 12mm and thickness of 2mm were tooled from mild steel rod, and further, these metal coupons were polished using increasing grades of emery papers 220, 400, 600, 1000 and then washed with Tap and distilled water and dried.

For electrochemical measurements, cylindrical test coupons with a surface area of 1.13cm^2 were tooled from a mild steel rod and further molded metallographically using the Acrylic cold setting resin. The exposed flat surface of the mounted metal was polished using various grades of emery papers (220, 400, 600, and 1000) and then polished on a disc polisher using a 1.0 micron levigated alumina abrasive.

Preparation of polymer coating

Preparation of acrylic resin

The hardener-to-softener ratio as 3:1 by volume or 2:1 by weight is taken. The mixture obtained is stirred until the desired consistency is achieved.

Preparation of Acrylic-Zinc Phosphate coating

To the above mixture, 0.32g of Zinc phosphate [$Zn_3(PO_4)_2$] is added to it to give 8% $Zn_3(PO_4)_2$. The mixture obtained is stirred until the desired consistency is achieved.

Preparation of nano-silver doped acrylic-$Zn_3(PO_4)_2$ coating

To the above mixture, add 0.003 g/L (to give 5 mM AgNPs). The mixture obtained is stirred until the desired consistency is achieved.

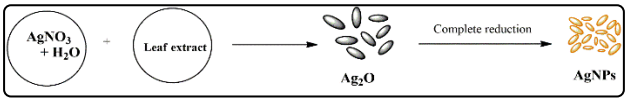

Fig. 1: Scheme of synthesis of AgNPs

Coating of a mild steel coupon

Manual coating is done over the polished metal coupons using the Spin coater (maintained at 1000rpm) and kept for drying. After drying, the coated metal coupons are kept for curing, by heating it in a water bath at around 78°C for half an hour and 88°C for one hour, with the continuous pressing of the coating.

Preparation of Silver nanoparticles (AgNPs)

The leaf powder (20g) of Ixora coccinea is taken in an RB flask with 100mL of water and heated at 60ºC for 20 minutes. It is then cooled for 2-3 hours and filtered using Whatmann filter paper. The filtrate is collected and kept aside. Further, to synthesize 5mM AgNPs, about 0.0849g of $AgNO_3$ is dissolved in 100mL of water and stirred thoroughly. In a dark room, 90mL of plant extract and 10mL of $AgNO_3$ solution are mixed in an ambered bottle and kept for incubation for 24 h. The formation of AgNPs was observed by the change of color from colorless to dark brown (Fig. 1).

Preparation of the media

The freshwater obtained from the laboratory is directly used as one of the mediums for corrosion studies on mild steel. Demineralized water is another corrosive medium taken for the study, which is obtained from Wation DB-100. The corrosion studies were done in a thermostat maintained at the required temperature.

Weight loss

The metal coupons were first polished using various grades of emery paper, 400, 600, and 1000, and then washed with tap water, and distilled water, and then dried, and further weighed and kept suspended in the respective corrosive medium. For the coated metal coupons, they were first polished, washed, dried, and then coated with the respective coating and kept for curing at 78°C for half an hour and 88°C for one hour with continuous pressing and drying, and kept in the respective medium. The loss in weight of the metal coupons is checked for a continuous interval of 3 days, and each time washing of the metal coupon with tap water and distilled water is done, dried, and

further, the weight is taken. The weight loss (g) can be calculated using Equation (1) and the corrosion rate can be calculated using Equation (2):

$$\text{Weight loss (g)}, \quad \Delta W = W_1 - W_2 \tag{1}$$

Where, W_1= Weight of the metal coupon before immersing in the medium, and W_2= Weight of the metal coupon after immersing in the medium

$$\text{Corrosion rate (mm/y)} = \frac{\Delta m \times 836}{A \rho t} \tag{2}$$

Where $\Delta m = W_2 - W_1$ (grams), W_1 = initial weight of the metal before being suspended in the corrosive liquid, Weight of the metal after removing the corrosive liquid, The surface area of the metal (cm^2), ρ = density of t he corroding metal/alloy (g/dm^3), t = time (days)

Estimation of the Chloride content in water

Chloride ion (Cl^-) is one of the major inorganic anions in water. The measured chloride content of the water can be tested to know the salinity of different water sources. Moreover, Chloride ion is one of the most penetrating ions, which could cause severe corrosion of the metal.

Standardization of $AgNO_3$ solution and Estimation of Chloride content in water

About 25 mL of prepared KCl solution or 25 mL of the water sample (normal water, demineralized water) is pipetted into a clean conical flask, with 10 drops of 2% K_2CrO_4 solution as the indicator. It is then titrated against 0.02N $AgNO_3$ solution in the burette. The endpoint is indicated by the appearance of a reddish-brown tinge which persists even after swirling the solution. The titration is repeated to get concordant values.

KCl reacts with $AgNO_3$ to form a curdy white precipitate of AgCl. Further, AgCl upon reaction with K_2CrO_4 forms a brick-red precipitate of Ag_2CrO_4.

$$KCl + AgNO_3 \longrightarrow AgCl + KCl$$

$$2AgNO_3 + K_2CrO_4 \longrightarrow Ag_2CrO_4 + 2KNO_3$$

The titration of AgCl vs $AgNO_3$ must be performed in a fresh medium since in the acidic medium, the CrO_4^{2-} ion changes to $Cr_2O_7^{2-}$ ion.

$$2CrO_4^{2-} + 2H^+ \rightleftharpoons Cr_2O_7^{2-} + H_2O$$

The weight of chloride as NaCl per liter of the solution is found by the equation (3):

$$X(g) = N_{Chloride} \times 58.5 \tag{3}$$

Where $N_{chloride}$ is the Strength (Normality) of Chloride in water.

The chloride content of the water sample is found by multiplying *W* by 1000 to obtain the chloride content in terms of ppm, given by Expression (4):

$$\text{Chloride content of water} = X \times 1000 \tag{4}$$

Estimation of Total Hardness of Water

The hardness of water is mainly caused due to the presence of dissolved salts, mostly calcium, magnesium, sulfates, carbonates, and bicarbonates. Hardness is expressed in parts of $CaCO_3$ equivalents parts per million (ppm) of water. Hard water results in the scaling of boilers, heat exchange units, cooling towers, and industrial equipment; by the precipitation of mineral forming deposits known as 'Scales', thereby reducing the efficiency and the life of the operating equipment. Therefore, the hardness of water is constantly monitored to avoid expensive breakdowns [20]. The standard method for the determination of water hardness is complexometric titration. Testing the hardness of water can provide information regarding if the water is potable or not.

Standardization of EDTA solution and Estimation of Hardness of Water

About 25mL of prepared Calcium carbonate solution (0.016M) or 25mL of water (freshwater, demineralized water) is pipetted out into a clean conical flask, and then 2-3ml of NH_4Cl-NH_4OH buffer solution is added, followed by adding 3 drops of Eriochrome Black-T indicator. The solution turns into a wine-red color. This solution is titrated against 0.002M EDTA taken in the burette. Indication of the endpoint is observed by the color change of the solution from wine red to blue. The titration is repeated to get concordant values.

From the weight of calcium carbonate, standardization, and estimation titer values the hardness can be calculated using Equation (6).

The weight of $CaCO_3$ in 25mL of a water sample can be calculated by the expression (5).

$$X(g) = \frac{W \times 1}{10 \times V_1} \times V_2 \tag{5}$$

Where, W(g)= Weight of $CaCO_3$, V_1= Volume of EDTA added (from standardization), V_2=Volume of EDTA added (From estimation)

The hardness of the water in terms of ppm can be calculated by the Expression (6):

$$\text{The hardness of water} = \frac{X \times}{25} 10^6 \text{ ppm} \tag{6}$$

Determination of pH

50mL of normal water is taken in a beaker. The standard sodium hydroxide (0.1N) solution is taken in a micro burette. The dual glass electrode is dipped in normal water and is connected to the pH meter. The initial pH of the normal water is noted. The titration is carried out by adding a minimum of 0.1mL sodium hydroxide. The strength of normal water can be determined by plotting the graph of pH along the y-axis and the volume of NaOH along the X-axis. The strength and pH of demineralized water are calculated by repeating the above experiment with 50 mL of demineralized water.

Electrochemical Measurements

The CH-Potentiostat of 600D-series purchased from the United States with beta software was connected to three electrodes with mild steel as an anode, saturated calomel electrode as a cathode, and inert platinum as a counter electrode. These three electrodes are kept in 100 mL of solution.

Electrochemical Impedance Spectroscopy (EIS)

In EIS, an AC signal of a small amplitude of 10 mV and a frequency sweep from 100000 Hz to 0.01 Hz was applied at the equilibrium potential and the resulting impedance data were analyzed using Nyquist plots. In both techniques, the readings of 2-3 trials were taken, and the average of the closing values was taken.

Potentiodynamic Polarisation Measurements (PPM)

The steady-state open circuit potentials concerning SCE were noted at the end of the 300s. The polarization studies were then studied from −250 mV to +250 mV with respective Open Circuit Potential (OCP) with a scan rate of 1 mV sec^{-1} and corresponding corrosion currents were recorded. PPM was carried out immediately after EIS, without further surface treatment. The readings are taken with and without the coatings. Inhibition efficiency and polarization potential were calculated from Stern-Geary equation (7) and equation (8) respectively.

$$\eta(\%) = \frac{i_{corr} - i_{corr(inh)}}{i_{corr}} \times 100 \quad (7)$$

Polarization potential

$$R_P = \frac{\beta a\, \beta c}{2.303(ba + bc)\, i(corr)} \quad (8)$$

Characterisation

FT-IR spectroscopy

Fourier transform infrared (FT-IR) spectrum of the Ixora coccinea was obtained using a Shimadzu - FT-IR 8400S spectrophotometer in the frequency sweep of 4000 to 400 cm^{-1} using the KBr pellet technique. The FT-IR analysis was carried out to identify the possible biomolecules responsible for the reduction of Ag^+ ions and capping of the bio-reduced nanoparticles synthesized by the aqueous leaf extract of Ixora coccinea.

UV-Spectroscopy

The formation of AgNPs was confirmed using the optical properties analysis through a UV-visible spectrophotometer.

Surface morphology

The coated and uncoated mild steel samples were exposed to the fresh and demineralized water separately for 3 days. Then the changes that occurred on the surface were evaluated by surface morphology studies using Scanning Electron Microscopy (SEM) and atomic force microscope (AFM).

Theoretical studies

Maestro Material Science, Schrodinger software was used to perform quantum chemical calculations, wherein the geometrical optimization for the acrylic tetramer was done using the Density Functional Theory (DFT) method. The hybrid functional with the correlational functional (B3LYP) and 6-31G++ as the basis set were chosen for the calculations. Furthermore, the energies of the highest occupied (E_{HOMO}) and lowest unoccupied (E_{LUMO}) molecular orbitals, electron affinity, and other parameters were calculated.

RESULTS AND DISCUSSION

Estimation of Chloride content of water

The chloride content for freshwater was found to be 2227 ppm and the chloride content for demineralized water was found to be 1425 ppm and is shown in Table 2.

pH measurement

The pH values for fresh water and demineralized water have been provided in Table 3.

The pH results revealed that freshwater has a lower pH than demineralized water. Therefore, mild steel corrodes more quickly due to the higher concentration of hydrogen ions in fresh water.

Table 2: Estimation of chloride content of water

Water sample	Standardization titre value (ml)	Estimation titre value (ml)	Weight of Chloride as NaCl per liter of the solution (X) (g)	The chloride content of water sample (ppm) = X × 1000
Freshwater	4.7	10	2.227	2227
Demineralized water	4.7	6.4	1.425	1425

The chloride content in demineralized water is less compared to freshwater (nearly 1000 ppm). Hence, freshwater is more reactive and corrosive.

Table 3: pH values of fresh water and demineralized water

Volume of NaOH (mL)	Fresh water (pH)	Demineralized water (pH)
0	6.85	6.66
0.1	10.4	7.41
0.2	10.71	7.44
0.3	10.74	7.45
0.4	10.75	7.48
0.5	10.79	7.48
0.6	10.82	7.49
0.7	10.84	7.52
0.8	10.85	7.54
0.9	10.86	7.56

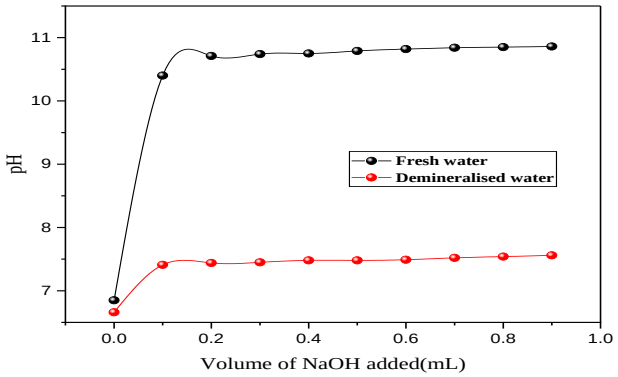

Fig. 2: pH values of fresh water and demineralized water at 303K

Table 2: Calculation of hardness of water samples

Water sample	Amount of $CaCO_3$ (g)	Standardization titer value (mL) (V_1)	Estimation titre value (mL) (V_2)	Weight of $CaCO_3$ in 25mL water sample X(g) = $\frac{W\times1}{10\times V_1}\times V_2$	Hardness = $\frac{X\times}{25}10^6$ (ppm)
Freshwater	0.16	21.3	1.7	0.000127	51
Demineralized ater	0.16	21.3	0.5	0.0003755	15

The hardness of fresh water is more in comparison to demineralized water. Hence corrosivity is more in fresh water.

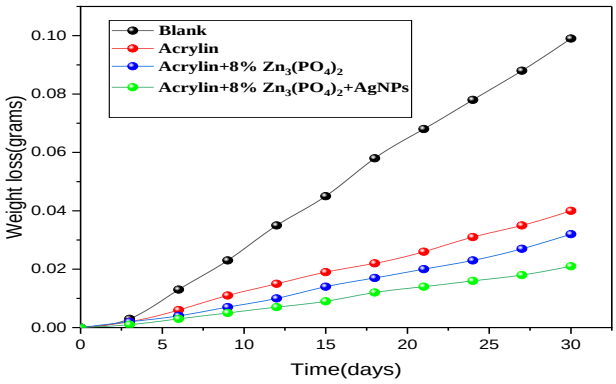

Fig. 2: Weight loss(g) vs. time(days) for coated and uncoated mild steel exposed to freshwater for 30 days.

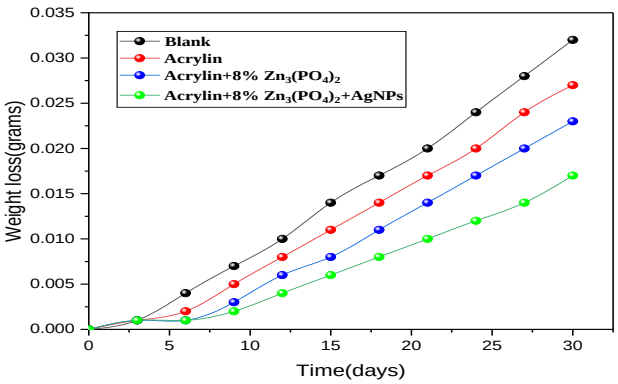

Fig. 3: Weight loss(g) vs. time(days) for coated and uncoated mild steel exposed to demineralized water for 30 days.

Weight loss measurements

The corrosion rate was calculated by measuring the weight of mild steel before and after dipping in fresh water and demineralized water with and without acrylic, acrylic+ 8% $Zn_3(PO_4)_2$, acrylic+ 8% $Zn_3(PO_4)_2$ +5mM AgNPs coatings for every 3 days up to 30 days by using the Equation (1). The weight loss data and corrosion rate data obtained for mild steel in fresh water and demineralized water at 303K are provided in Tables 3 and 4 respectively.

Hardness of water

The estimated hardness of freshwater and demineralized water was found to be 51ppm and 15ppm respectively. The results are tabulated in Table 2.

Figs. 2 and 3 show the plot of weight loss (g) vs. Time (days) obtained for the coated and uncoated mild steel in fresh water and demineralized water respectively.

From Figs. 2 and 3, it is quite evident that the weight loss of mild steel in freshwater gradually increases with

Table 3: Weight loss data for mild steel in freshwater with and without coating at 303K

No of days	Parameter	Blank	Acrylic	Acrylic + 8%$Zn_3(PO_4)_2$	Acrylic + 8%$Zn_3(PO_4)_2$ + AgNPs
3	Weight loss(g)	0.003	0.002	0.002	0.001
	Corrosion rate(mm/y)	0.061214	0.040809	0.040809	0.020405
6	Weight loss(g)	0.013	0.006	0.004	0.003
	Corrosion rate(mm/y)	0.132631	0.061214	0.040809	0.030607
9	Weight loss(g)	0.023	0.01	0.007	0.005
	Corrosion rate(mm/y)	0.156436	0.068016	0.047611	0.034008
12	Weight loss(g)	0.035	0.014	0.01	0.007
	Corrosion rate(mm/y)	0.178541	0.071416	0.051012	0.035708
15	Weight loss(g)	0.045	0.018	0.013	0.009
	Corrosion rate(mm/y)	0.183642	0.073457	0.053052	0.036728
18	Weight loss(g)	0.058	0.022	0.016	0.011
	Corrosion rate(mm/y)	0.197246	0.074817	0.054413	0.037409
21	Weight loss(g)	0.068	0.026	0.019	0.013
	Corrosion rate(mm/y)	0.198217	0.075789	0.055384	0.037894
24	Weight loss(g)	0.078	0.03	0.022	0.015
	Corrosion rate(mm/y)	0.198946	0.076518	0.056113	0.038259
27	Weight loss(g)	0.088	0.034	0.025	0.017
	Corrosion rate(mm/y)	0.199513	0.077084	0.05668	0.038542
30	Weight loss(g)	0.099	0.039	0.028	0.019
	Corrosion rate(mm/y)	0.202007	0.079578	0.057133	0.038769

Table 4: Weight loss data for mild steel in demineralized water with and without coating at 303K

No of days	Parameter	Blank	Acrylic	Acrylic + 8%$Zn_3(PO_4)_2$	Acrylic + 8%$Zn_3(PO_4)_2$ + AgNPs
3	Weight loss(g)	0.001	0.001	0.001	0.001
	Corrosion rate(mm/y)	0.0204	0.0204	0.0204	0.0204
6	Weight loss(g)	0.004	0.002	0.001	0.001
	Corrosion rate(mm/y)	0.04081	0.0204	0.0204	0.0204
9	Weight loss(g)	0.007	0.005	0.003	0.002
	Corrosion rate(mm/y)	0.04761	0.03401	0.0204	0.0204
12	Weight loss(g)	0.01	0.008	0.006	0.004
	Corrosion rate(mm/y)	0.05101	0.04081	0.03061	0.0204
15	Weight loss(g)	0.014	0.011	0.008	0.006
	Corrosion rate(mm/y)	0.05713	0.04489	0.03265	0.02449
18	Weight loss(g)	0.017	0.014	0.011	0.008
	Corrosion rate(mm/y)	0.05781	0.04761	0.03741	0.02721
21	Weight loss(g)	0.02	0.017	0.014	0.01
	Corrosion rate(mm/y)	0.0583	0.04955	0.04081	0.02915
24	Weight loss(g)	0.024	0.02	0.017	0.012
	Corrosion rate(mm/y)	0.06121	0.05101	0.04336	0.03061
27	Weight loss(g)	0.028	0.024	0.02	0.014
	Corrosion rate(mm/y)	0.06348	0.05441	0.04534	0.03174
30	Weight loss(g)	0.032	0.027	0.023	0.017
	Corrosion rate(mm/y)	0.0653	0.05509	0.04693	0.03469

an increase in the number of days of exposure to the metal. This may be due to, continuously exposing the metal to the water medium, more and more polar water molecules or charged ions present in the water will be

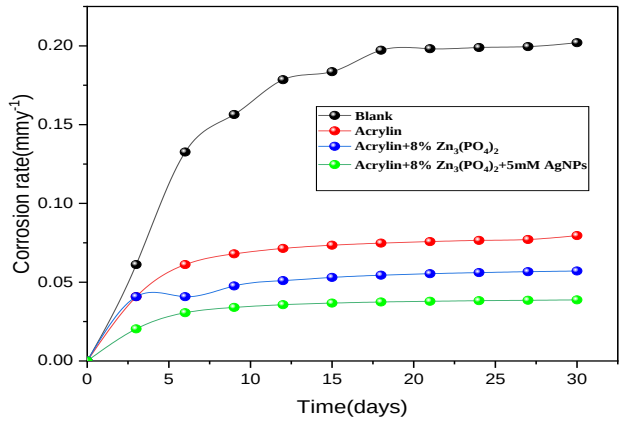

Fig. 4: Corrosion rate (mm/y) vs. time (in days) for mild steel exposed to freshwater

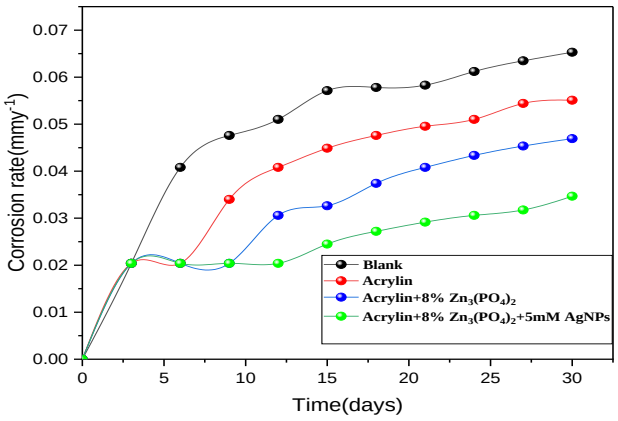

Fig. 5: Corrosion rate (mm/y) vs. time (days) for mild steel exposed to demineralized water

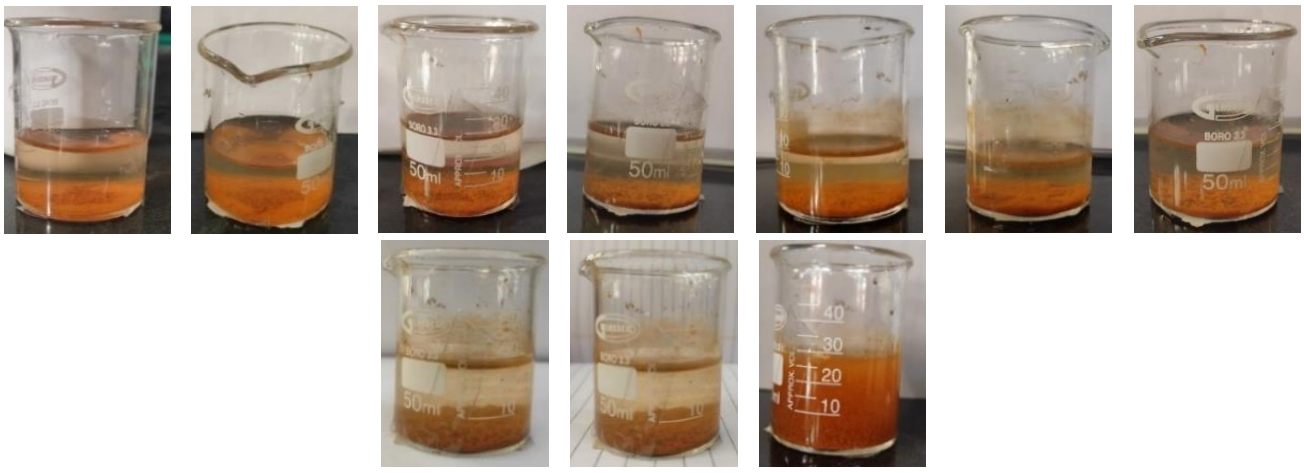

Fig. 6: The photo of freshwater containing mild steel exposed for 30 days.

adsorbed on the metal surface. These adsorbed charged species will stimulate the creation of more active centers on the metal, thereby increasing the metal reactivity and promoting the corrosion process.

By using acrylic coating there will be a drastic decrease in weight loss and corrosion rate. This acrylic polymer blocks most of the active centers. Hence, a polymer barrier is created between the metal and the environment (corrosive medium). However, this polymer coating is not suitable for long-term exposure, as it has a large number of pores, through which water molecules make a way to adsorb on the metal. The introduction of 8% $Zn_3(PO_4)_2$ as a filler, increases the force of attraction between the polymer molecules, thereby decreasing the number of interstitial positions or spaces. Hence, water absorption decreases. This effect is further increased by adding AgNPs to acrylic with 8% Zinc phosphate. This may be due to silver increasing the force of attraction between the acrylic molecules and decreasing its disbonding tendency.

The weight loss or corrosion rate is higher in freshwater compared to demineralized water, as it contains a greater number of charged ions.

Figs. 4 and 5 represent the plot of corrosion rate (mm/y) of mild steel vs. time (in days) in fresh water and demineralized water respectively.

From the graphs, it has been observed that the corrosion rate increases with an increase in the number of days of exposure of the metal to the corrosive medium. The images of the solution containing mild steel with and without acrylic, acrylic + 8% $Zn_3(PO_4)_2$, and acrylic+ 8% $Zn_3(PO_4)_2$ + 5mM AgNPs for 30 days are shown in Figs. 6, 7, 8, 9 for fresh water and Figs. 10, 11, 12, 13 for demineralized water respectively.

Potential and corrosion current values

The potential and current values were calculated using a multimeter by dipping the metal in fresh water and demineralized water with and without different

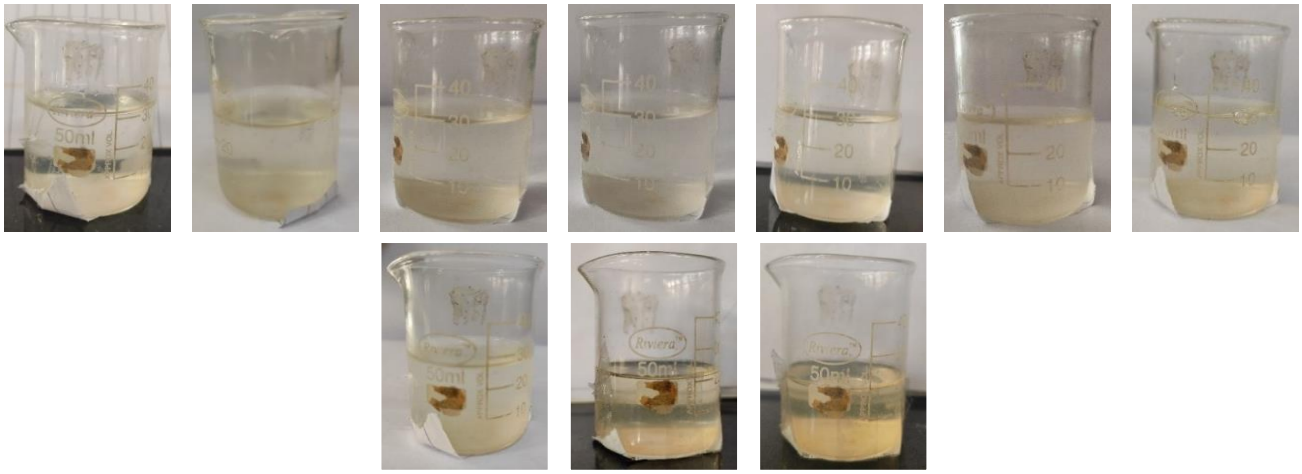

Fig.7: The photos of fresh water containing Acrylic coated mild steel exposed for 30 days.

Fig. 8: The photos of fresh water containing Acrylic + 8% $Zn_3(PO_4)_2$ coated mild steel for 30 days.

Fig. 9: Photos of fresh water containing Acrylic + 8% $Zn_3(PO_4)_2$ + 5mM AgNPs coated mild steel exposed for 30 days.

coatings every 3 days up to 30 days and noting down the values. The potential and current values obtained for mild steel in fresh water and demineralized water at 303K are provided in Tables 5 and 6.

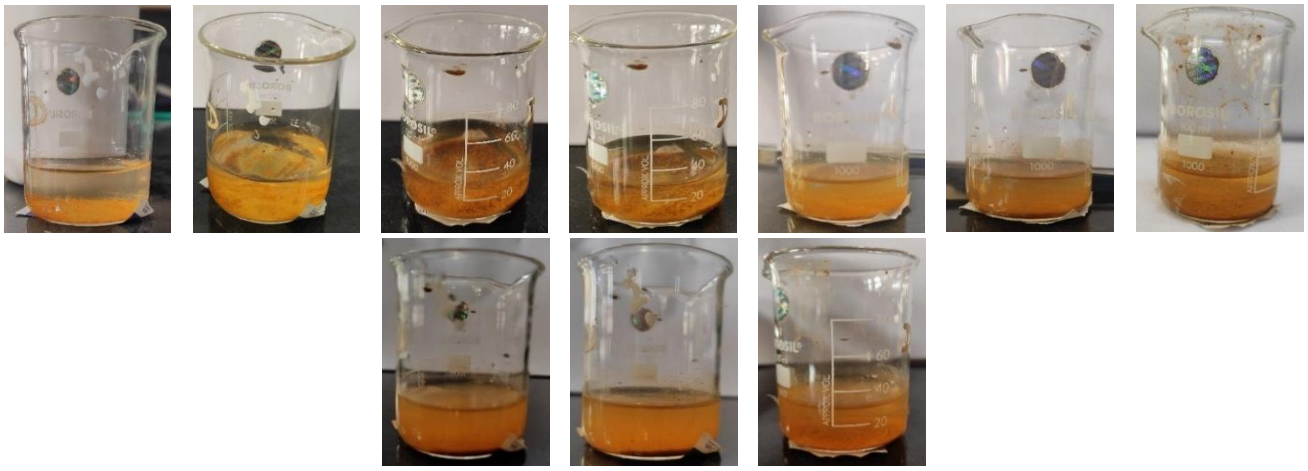

Fig. 10: The photo of demineralised water containing mild steel exposed for 30 days.

Fig. 11: The photos of demineralised water containing Acrylic coated mild steel exposed for 30 days.

Fig. 12: The photos of demineralized water containing Acrylic + 8% $Zn_3(PO_4)_2$ coated mild steel for 30 days.

From the plot, it was observed that with the increase in time of exposure, there will be an increase in the corrosion potential and current. When the metal is continuously in contact with the medium the anions, cations, and polar water molecules are adsorbed on the surface. These ions stimulate the reactive mild steel surface to continuously

Fig. 13: Photos of demineralised water containing Acrylic + 8% $Zn_3(PO_4)_2$ + 5mM AgNPs coated mild steel exposed for 30 days.

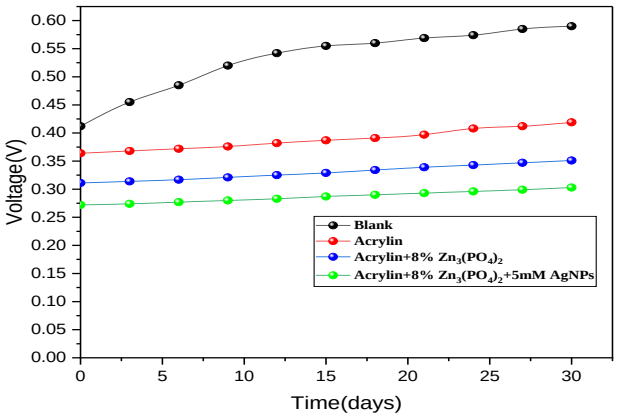

Fig. 14: Voltage(V) vs Time(days) for coated and uncoated mild steel in freshwater for 30 days

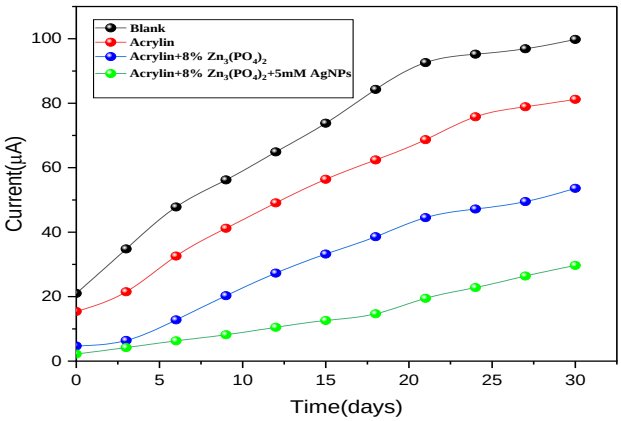

Fig. 16: Current(μA) vs. Time(days) for coated and uncoated mild steel in fresh water for 30 days

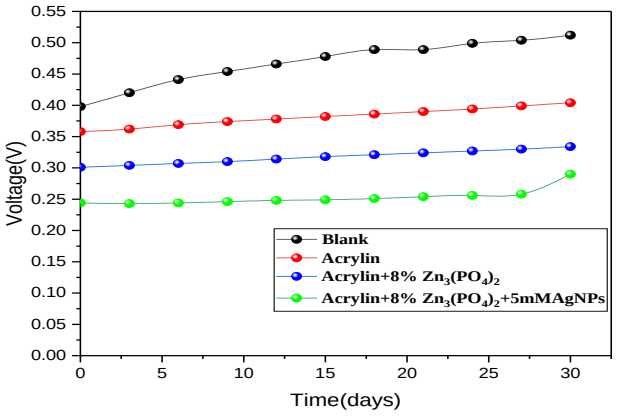

Fig. 15: Voltage(V) vs Time(days) for coated and uncoated mild steel in demineralized water for 30 days

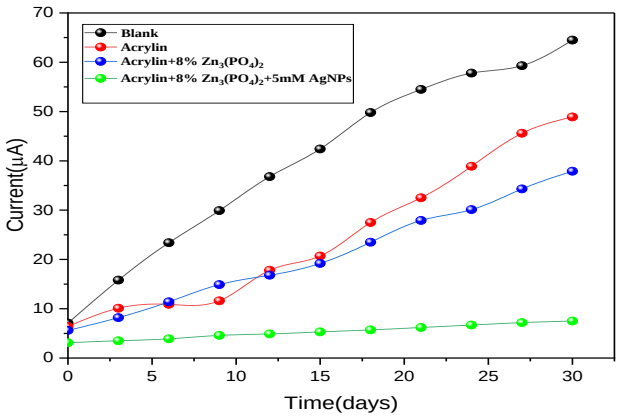

Fig. 17: Current(μA) vs. Time(days) for coated and uncoated mild steel in demineralized water for 30 days.

dissolve, and an exchange of charge takes place between the metal and medium.

By applying the coating, the potential and current values are reduced. That is because the coating forms a barrier between the metal and the environment. The strength of the coating is increased by adding 8% $Zn_3(PO_4)_2$ to acrylic polymer and it also forms a passive film, thereby further decreasing the rate of corrosion. The force of attraction is

Table 5: Voltage and current values for coated and uncoated mild steel in freshwater

No of days	Parameter	Blank	Acrylic	Acrylic + 8% $Zn_3(PO_4)_2$	Acrylic + 8%$Zn_3PO_4)_2$ + 5mMAgNPs
0	Voltage(V)	0.412	0.364	0.311	0.272
	Current(µA)	21.0	15.4	4.7	2.2
3	Voltage(V)	0.455	0.368	0.314	0.274
	Current(µA)	34.8	21.5	6.4	4.2
6	Voltage(V)	0.485	0.372	0.317	0.277
	Current(µA)	47.8	32.6	12.8	6.3
9	Voltage(V)	0.52	0.376	0.321	0.28
	Current(µA)	56.2	41.2	20.3	8.2
12	Voltage(V)	0.542	0.382	0.325	0.283
	Current(µA)	64.9	49.1	27.3	10.5
15	Voltage(V)	0.555	0.387	0.329	0.287
	Current(µA)	73.8	56.4	33.2	12.6
18	Voltage(V)	0.56	0.391	0.334	0.29
	Current(µA)	84.3	62.4	38.6	14.7
21	Voltage(V)	0.569	0.397	0.339	0.293
	Current(µA)	92.6	68.7	44.5	19.5
24	Voltage(V)	0.574	0.408	0.343	0.296
	Current(µA)	95.2	75.8	47.2	22.8
27	Voltage(V)	0.585	0.412	0.347	0.299
	Current(µA)	96.9	78.9	49.5	26.4
30	Voltage(V)	0.59	0.419	0.351	0.303
	Current(µA)	99.8	81.2	53.6	29.7

further increased by adding 5mM to acrylic and 8% $Zn_3(PO_4)_2$. That is due to the increase in the force of attraction and the decrease in the disbonding nature of the acrylic polymer.

Potentiodynamic polarization results

Valuable potentiometric polarization parameters like corrosion current density ($i_{Corr.}$), corrosion potential ($E_{corr.}$), and anodic and cathodic Tafel slopes (β_a, $-\beta_c$) were obtained from the Tafel plots. Which is a plot of Potential vs logi.

The point where the anodic polarization curve and cathodic polarization meet gives the corrosion current ($i_{corr.}$). The linear part of anodic and cathodic polarization curves gives the anodic(b_a) and cathodic Tafel slopes($-b_c$). The corrosion current density, anodic and cathodic Tafel slopes, and corrosion rate are obtained from the potentiodynamic plots. The results obtained for mild steel on exposure to fresh water and Demineralised water for 3 days at 303K, 313K, and 323K are tabulated in Tables 7 and 8. Fig. 18 and 19 represent the Potentiodynamic plots for the mild steel on exposure to fresh water and demineralized water for 3 days, respectively at 303K and 313K. Similar plots are obtained at 323K.

From the results obtained it was observed that the corrosion rate and corrosion current density increase with an increase in temperature. This may be because, with the increase in temperature, the conductivity of the medium increases, and the number of active centers on the mild steel surface increases. Hence, an increase in metal dissolution occurs.

By applying acrylic coating most of the active centers are blocked and hence there is a decrease in corrosion rate and corrosion current density.

As seen, after applying coating a significant decline in both cathodic and anodic currents was noticed, suggesting that the acrylic coating with carboxylic acid functional group locks the active centers at the anode and cathode. The results also show that the inhibition efficiency increased, while the corrosion current density of mild steel from 2.89 µA/cm^2

Table 6: Voltage and current value for coated and uncoated mild steel in demineralized water

No of days	Parameter	Blank	Acrylic	Acrylic + 8% $Zn_3(PO_4)_2$	Acrylic + 8%$Zn_3(PO_4)_2$ + 5mM AgNPs
0	Voltage(V)	0.398	0.358	0.301	0.244
	Current(μA)	7.1	6.4	5.6	3.1
3	Voltage(V)	0.42	0.362	0.304	0.243
	Current(μA)	15.8	10.1	8.2	3.5
6	Voltage(V)	0.441	0.369	0.307	0.244
	Current(μA)	23.4	10.9	11.4	3.9
9	Voltage(V)	0.454	0.374	0.31	0.246
	Current(μA)	29.9	11.6	14.9	4.6
12	Voltage(V)	0.466	0.378	0.314	0.248
	Current(μA)	36.8	17.8	16.8	4.9
15	Voltage(V)	0.478	0.382	0.318	0.249
	Current(μA)	42.4	20.7	19.2	5.3
18	Voltage(V)	0.489	0.386	0.321	0.251
	Current(μA)	49.8	27.5	23.5	5.7
21	Voltage(V)	0.489	0.39	0.324	0.254
	Current(μA)	54.5	32.5	27.9	6.2
24	Voltage(V)	0.499	0.394	0.327	0.256
	Current(μA)	57.8	38.9	30.1	6.7
27	Voltage(V)	0.504	0.399	0.33	0.258
	Current(μA)	59.3	45.6	34.3	7.2
30	Voltage(V)	0.512	0.404	0.334	0.29
	Current(μA)	64.5	48.9	37.9	7.5

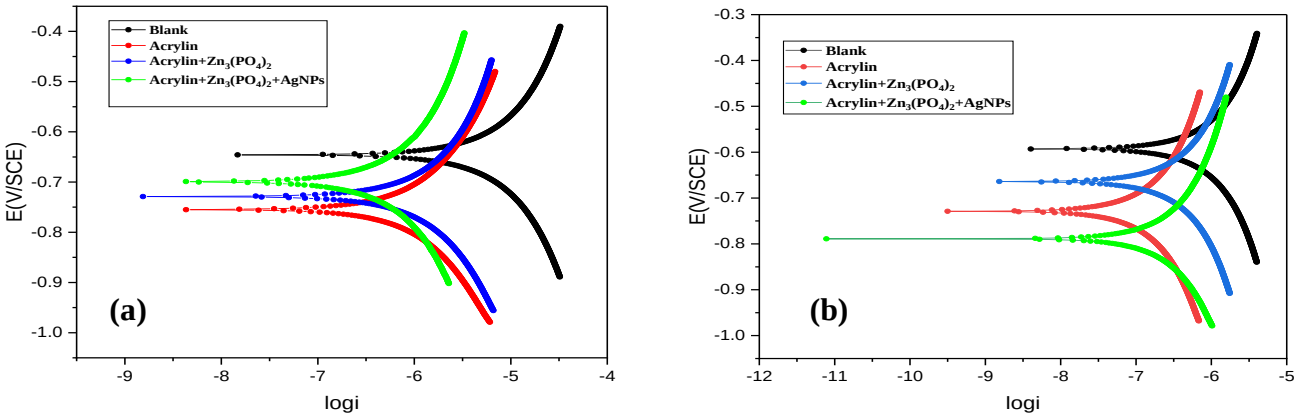

Fig. 18 (a): Potentiodynamic plots for corrosion of mild steel (with and without coating) in (a) freshwater and (b) Demineralised water at 303K.

to 0.000000421A cm^{-2} decreased and increased the corrosion coating efficiency to 81%. This behavior is because of the excellent coverage of the metal surface by an acrylic coating which blocked the reaction sites on the metal surface. The corrosion current density is drastically decreased by introducing 8% $Zn_3(PO_4)_2$ in the acrylic coating. Zinc phosphate increases the force of attraction between acrylic polymer, thereby not allowing the corroding ions, and molecules to enter inside through the coating. Hence increased coating efficiency is observed. This effect is further increased by introducing 5mM of nanosilver (AgNPs) to the acrylic coating with 8% zinc phosphate.

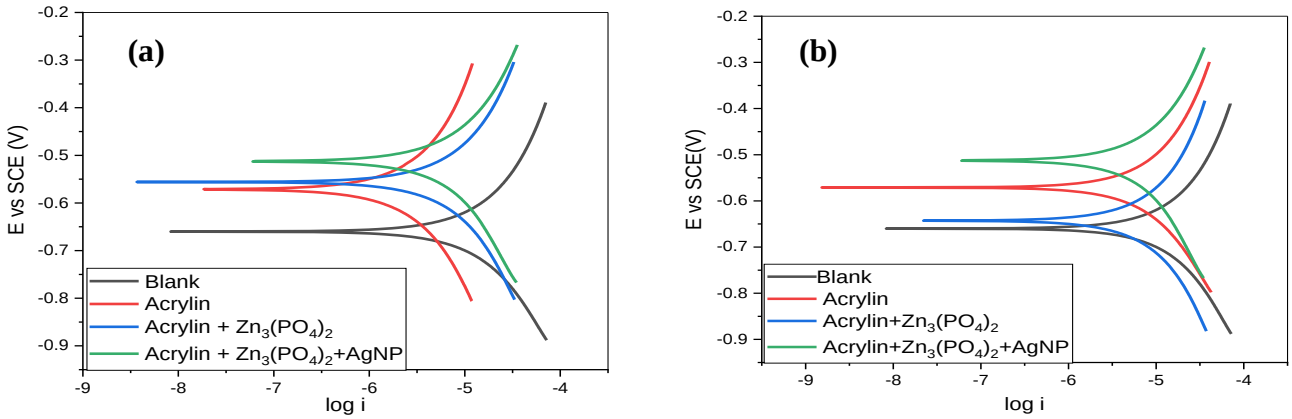

Fig. 18(b): Potentiodynamic plots for corrosion of mild steel (with and without coating) in (a) Freshwater and (b) Demineralised water at 303K

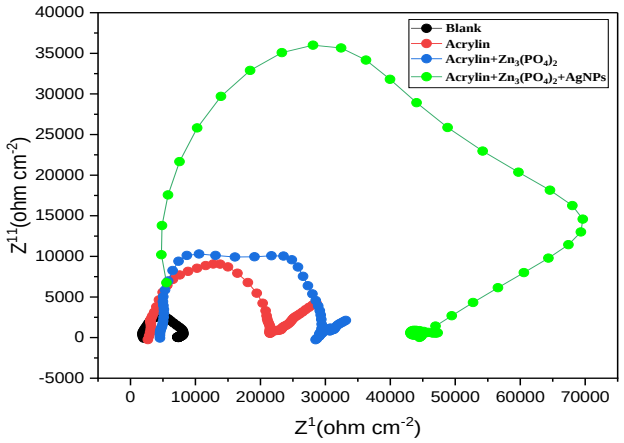

Fig. 20: Nyquist plot for corrosion of mild steel in fresh water at 303K

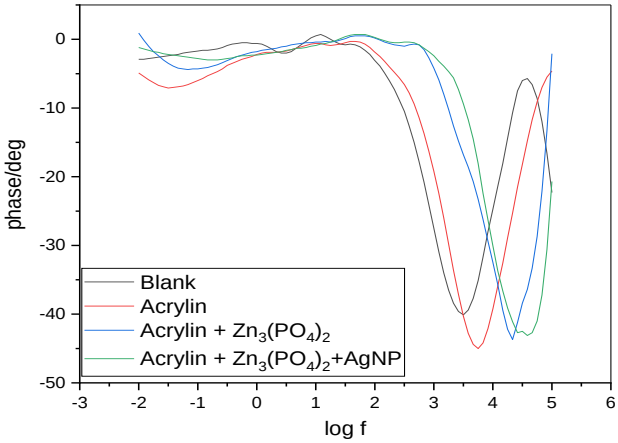

Fig. 21: Bode plot for corrosion of mild steel in fresh water at 303K

There is no change in anodic and cathodic Tafel slopes by changing the temperature [3750]. This suggests that an increase in temperature does not change the steps involved in the anodic and cathodic reactions. The similar values indicate that temperature increases the surface area available for corrosion, thereby increasing corrosion.

There is a +22mV change in corrosion potential with the increase of temperature for mild steel in freshwater. According to *Li et al*., the increase in temperature favors both the anodic reaction and oxygen absorption [21].

With the introduction of coating, the maximum displacement of more than -85 mV in corrosion potential was observed. These insights that the blocking effect of acrylic and its filler is more at the cathode compared to the anode.

With the increase of temperature, coating efficiency decreased, which shows an adsorbing tendency of the acrylic coating decreases, the corroding tendency of outside water increases due to a decrease in viscosity of the medium or no active centers are increased due to an increase in conductivity of mild steel. The combined effect of all or any one-two effect may be dominating with the increase in temperature [22-23].

Electrochemical impedance spectroscopy

Fig. 20 represents the plot obtained by taking an imaginary part of impedance on the Y-axis and the real part of impedance on the X-axis for the corrosion of mild steel with and without coating. Fig .21 represents the Bode plot as observed from Fig. 20, the shape of the curves is half-circle, which implies that the transfer of charges takes place between mild steel and freshwater.

The semi-circles were diminished, this may be due to, non-homogeneity on the metal surface causing the variation in frequency. The non-homogeneity may be due

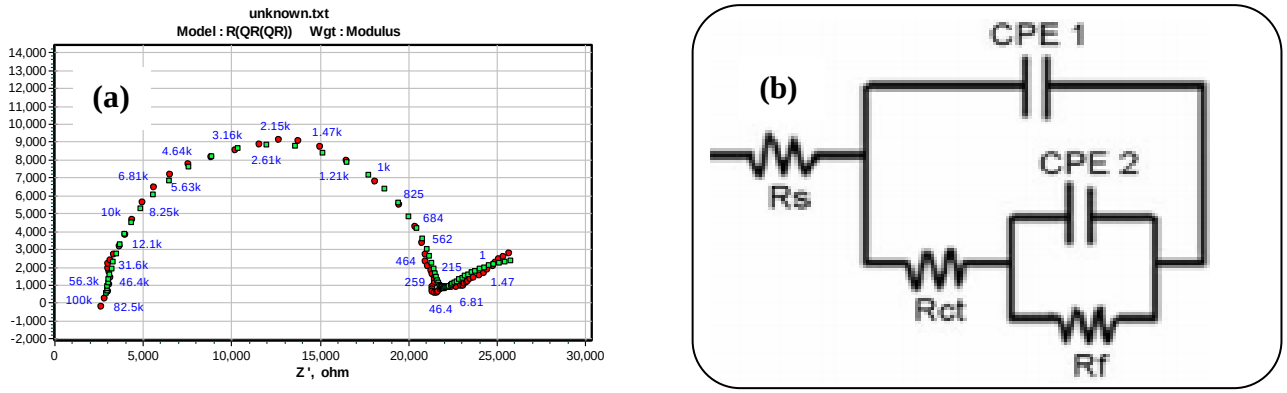

Fig. 22: (a) Impedance data fitted for mild steel in fresh water at 303K. (b) Equivalent circuit.

to the deposition of ferric oxide, or other ions on the mild steel surface. The semi-circle diameter represents the resistance to the exchange of ions at the mild steel-fresh/demineralized water interface (R_{ct}). With the increase in temperature, the diameter of semicircles decreases, this observation may be due to the increase in the mobility of ions of fresh water and reactivity of the mild steel surface, with the increase in temperature.

By applying the coating, there will be an increase in the diameter of the semicircle. This shows that acrylic coating forms the barrier between the metal and the environment. The barrier effect is enhanced by introducing 8% $Zn_3(PO_4)_2$ and 5 mM AgNPs to acrylic coating. This is confirmed by the C.E., values obtained by R_p values, which were obtained by fitting the impedance parameters to a suitable equivalent circuit.

With the increase of temperature, I.E., decreased, that shows a decrease in the adsorbing tendency of the acrylic coating does not efficiently decrease the charge transfer at the metal solution interface, or increased charges at the double layer due to a decrease in viscosity of the medium, or the number of reactive sites is increased due to increase in conductivity of mild steel. The combined effect of all or any one effect may be dominating with the increase in temperature.

The Nyquist plots are evaluated by applying the impedance Excel data to the Zimpwin software 3.21 to get the appropriate equivalent circuits. The satisfactory equivalent circuit having a minimal Zai factor is shown in Fig. 22(b), and fitted curves are shown in Fig. 22(a).

R_s is the resistance offered by the solution present between anode and cathode, Constant Phase Element 1 (CPE 1), the electrical double layer dielectric constant, CPE 2 capacitance of the passive ferric oxide film, and R_f film resistance. Due to the irregular surface, the charged layer present on the mild steel surface and water boundary is not a perfect capacitor. Hence it is replaced by CPE [24-25].

The CPE impedance is calculated using Equation (9):

$$Z= Q^{-1} (iw)^{-n} \quad (9)$$

The *Q* is the proportionality coefficient; $w=2\pi f_{max}$ is the angular frequency; f_{max} is the frequency at which the imaginary component of the impedance is maximum, *i* is the imaginary number, and the power *n* is associated with the phase shift. If n = 1, then the charged double layer at the boundary behaves like an ideal capacitor. The correction in the capacitance to its real value is calculated using Equation (10).

$$C_{dl} = Q(w)^{n-1} \quad (10)$$

The C_{dl} at the mild steel water with and without coatings was evaluated using (11).

$$C_{dl} = \frac{1}{2\pi f_{max} R_P} \quad (11)$$

The polarization resistance *Rp* at the mild steel-water with and without coatings was calculated using (12).

$$R_p = R_{ct} + R_f + R_s \quad (12)$$

From Fig. 22, it is observed that R_s with and without coating in water have the nearly same value. By introducing acrylic coating on mild steel R_p value rises, and C_{dl} values suppress. It confirms the blocking of active centers present on mild steel surfaces by the molecules of acrylic. The coating effect of acrylic was enhanced by adding zinc phosphate and silver nanoparticles. At the mild steel surface and water interface net exchange of charges decreases (resistance to charge transfer R_{ct} increases) and the thickness of the electrical double layer increases due to the presence of coated big polymer molecules. Therefore, by introducing acrylic coating capacitance rises, and

Table 7: Potentiodynamic polarization measurements for mild steel in freshwater for 3 days.

Temp. (K)	Freshwater	$i_{Corr.}$	C.R. (mm/y)	b_a (mV/dec)	$-b_c$ (mV/dec)	$E_{corr.}$ (mV vsSCE)	I.E (%)	R_p (ohm cm^2)	C_{dl} (10^{-10} F/cm^2)	I.E (%)
303	Blank	4.99	1.138	4.999	4.896	-0.646	-	9937	61.09	-
	Acrylic coating	0.666	0.1636	5.322	5.399	-0.755	87	31231	5.72	68
	Ac/Zn coating	0.312	0.1365	4.888	5.274	-0.729	93	48847	0.412	80
	Ac/Zn/AgNPs	0.197	0.0585	5.009	4.966	-0.699	96	168847	0.262	94
313	Blank	6.526	1.417	4.910	4.972	-0.589	-	7969	78.4	-
	Acrylic coating	0.980	0.1904	5.170	5.212	-0.762	84	24174	6.21	66
	Ac/Zn coating	0.573	0.152	4.588	4.992	-0.742	91	36256	0.059	78
	Ac/Zn/AgNPs	0.49	0.0754	4.891	5.095	-0.653	92	88206	0.381	91
323	Blank	8.22	1.719	5.221	5.848	-0.552	-	5640	89.8	-
	Acrylic coating	1.371	0.2171	6.254	6.123	-0.629	83	16213	7.04	65
	Ac/Zn coating	0.838	0.1734	5.984	5.987	-0.529	89	24995	0.696	75
	Ac/Zn/AgNPs	0.660	0.0893	6.244	5.678	-0.499	91	50801	0.471	88

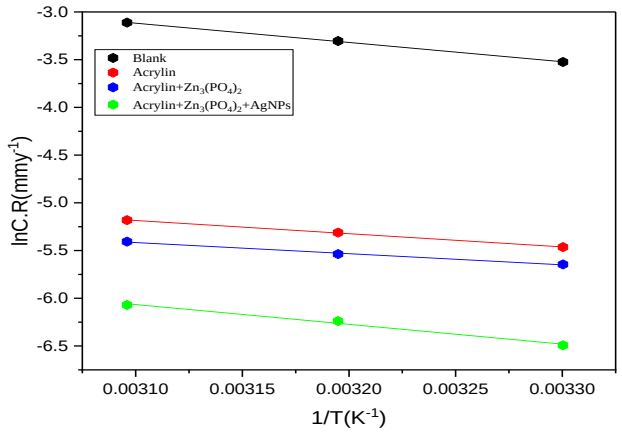

Fig. 23: Arrhenius plots for corrosion of mild steel with and without coatings in fresh water at 303K, 313K, and 323K

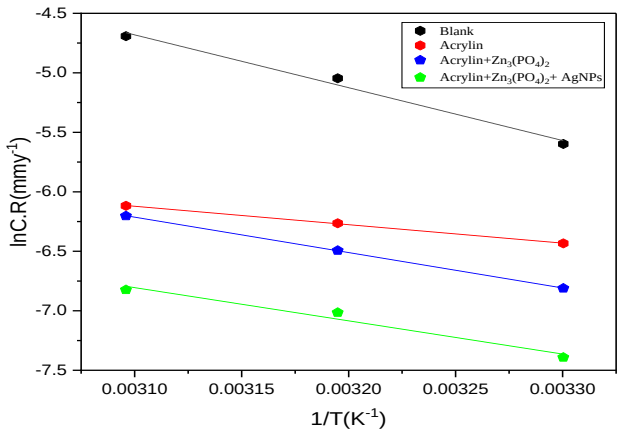

Fig. 24: Arrhenius plots for corrosion of mild steel with and without coatings in demineralized water at 303K, 313K, and 323K

resistance to shifting equilibrium potential from the net corrosion current (Rp) rises at the mild steel and water interface increases. By adding zinc phosphate to acrylic coating water adsorbing property was decreased and bonding tendency increased. [24-25]. The impedance parameters are given in Tables 7 and 8.

The R_p is used to calculate the % I.E., using equation (13).

$$\%C.E.=\frac{R_{P(coating)}-R_P}{R_{P(coating)}} \quad (13)$$

Where $R_{p(coating)}$ and R_p are with and without coatings in water, respectively.

Consequences of change of thermostat Temperature

The relationship between temperature and corrosion of mild steel and its inhibition by applying the coatings can be followed by applying the Arrhenius rate law (14) and transition state Equation (15) for the corrosion rate values obtained by Potentiodynamic polarization measurements.

$$\ln (CR)=Ae^{\frac{-E_a}{RT}} \quad (14)$$

Where A is an Arrhenius pre-exponential factor; R= 8.314 J/mol.K, T= thermostat temperature. Plots of ln (C.R.) against 1/T gives a linear curve, and from -slope×R, the energy of activation E_a was calculated.

Table 9 shows the values of activation energy in the presence and absence of coating. Activation energy gives information about the energy needed to cross the barrier from reactants to products, in other words, it represents the minimum energy needed to start the corrosion reaction.

$$CR = (\frac{RT}{Nh})e^{\frac{\Delta S_a}{R}}e^{-\frac{\Delta H_a}{RT}} \quad (16)$$

Where, h = 6.626×10^{-34} Js and N =6.023×10^{23}.

Plots of ln (CR/T) versus 1/T for the corrosion of mild steel in fresh water and demineralized water medium containing different coatings are shown in Figs. 25 and 26.

Table 8: Potentiodynamic polarization measurements for mild steel in demineralized water

Temp. (K)	Demineralized water	$i_{Corr.}$ (A/cm^2)	C.R. (mm/y)	b_a (mV dec^{-1})	-b_c (mVdec^{-1})	$E_{corr.}$ (mV vs SCE)	I.E (%)	R_p (ohm cm^2)	C_{dl} (10^{-10} $_{Fcm}^{-2}$)	I.E (%)
303K	Blank	2.89	0.1431	4.922	4.948	-0.593	-	21410	2.94	-
	Acrylic coating	0.421	0.0620	4.964	5.044	-0.729	85	114267	0.09403	81
	Ac/Zn coating	0.563	0.0425	4.889	5.009	-0.664	91	318751	0.0386	93
	Ac/Zn/AgNPs	0.2002	0.0232	4.920	5.131	-0.789	93	453235	0.00638	95
313K	Blank	4.34	0.2485	4.921	4.999	-0.576	-	18960	3.69	-
	Acrylic coating	0.696	0.0734	4.930	4.988	-0.761	83	92535	0.1021	79
313K	Ac/Zn coating	0.432	0.0584	4.850	4.872	-0.673	90	197019	0.0497	90
	Ac/Zn/AgNPs	0.3524	0.0347	4.922	5.289	-0.768	91	331503	0.00768	94
323K	Blank	5.595	0.3539	4.923	5.134	-0.568	-	16510	4.72	-
	Acrylic coating	0.9876	0.08512	4.929	5.064	-0.776	82	55560	0.11323	70
	Ac/Zn coating	0.6289	0.07187	4.897	5.008	-0.684	88	134484	0.0586	87
	Ac/Zn/AgNPs	0.5014	0.0420	4.978	5.145	-0.713	90	268968	0.00898	93

Table 9: Activation parameters for mild steel in freshwater with and without coatings

Concentration (g/L)	E_a (kJ/mol)	ΔH_a (kJ/mol)	ΔS_a (kJ/mol.K)
0	16786.5	14816.5	-227.50
3.0g/L Acrylic	11496.5	8934.3	-260.96
3.0g/L Acrylic+0.24 $Zn_3(PO_4)_2$ g/L	9686	7098.2	-268.58
3.0 Acrylic+0.24 $Zn_3(PO_4)_2$ g/L+ 0.084 g/L AgNPs	17239.07	14856.2	-249.214

Table 10: Activation parameters for mild steel in demineralized water with and without coatings

Concentration (g/L)	E_a (kJ/mol)	ΔH_a (kJ/mol)	ΔS_a (kJ/mol.K)
0	36911.66	34311.04	-216.9
3.0 g/L Acrylic	12879.13	10278.59	-264.59
3.0 g/L Acrylic + 0.24 g/L $Zn_3(PO_4)_2$	24737.8	18756.3	-239.634
3.0 g/L Acrylic + 0.24 g/L$Zn_3(PO_4)_2$ + 0.084 g/L AgNPs	23209.36	21516.63	-235.41

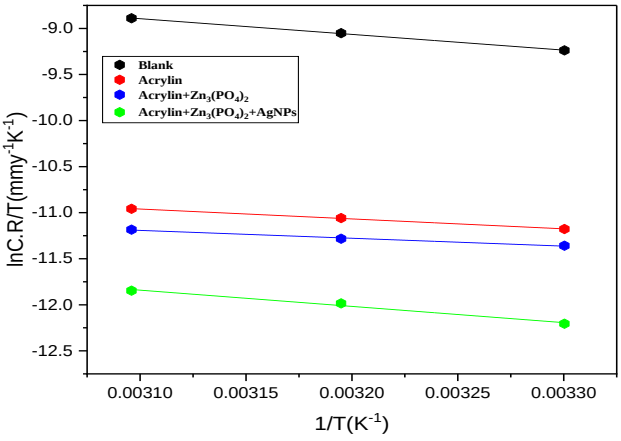

Fig. 25: Plots of ln (CR/T) vs. 1/T for mild steel in freshwater with and without coatings at 303K, 313K, and 323K

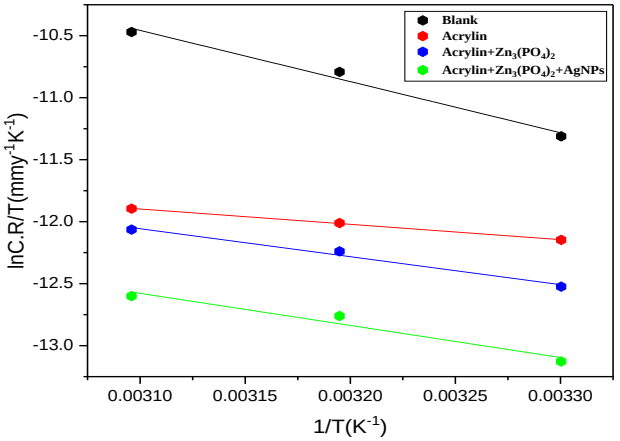

Fig. 26: Plots of ln (CR/T) vs. 1/T for mild steel in demineralized water with and without coatings at 303K, 313K, 323K

Plots of ln (CR/T) against 1/T give a linear curve and from -slope×R and [Intercept- $\frac{lnR}{Nh}R$ enthalpy of activation (ΔH_a) and entropy of activation (ΔS_a) were calculated respectively. The energy values are summarized in Tables 9 and 10.

By applying acrylic coating on mild steel, Activation energy (E_a) values rise. It may be due to the active center reactivity nullified by the acrylic coating, raising the energy barrier for the electrochemical reaction taking place

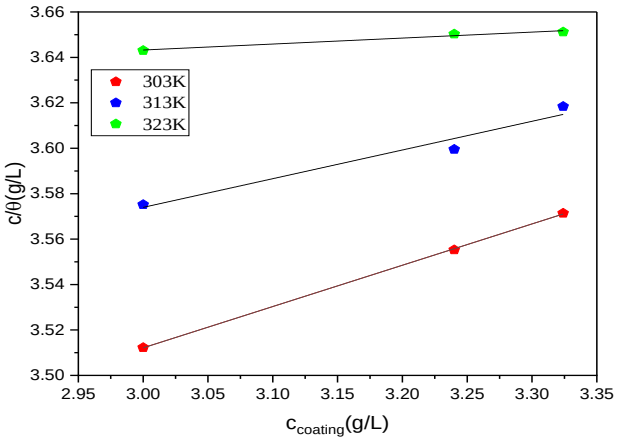

Fig. 27: Langmuir adsorption isotherms for acrylic coating on mild steel in freshwater

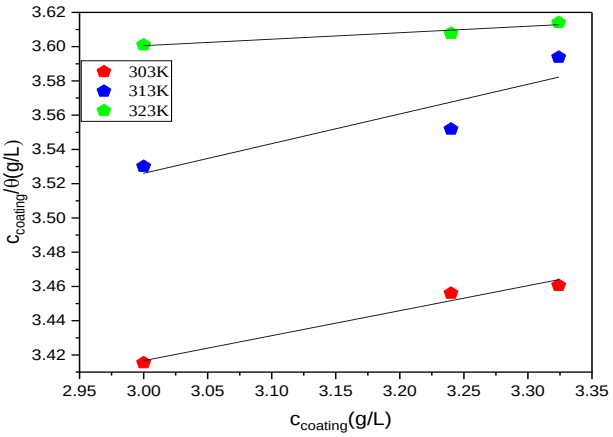

Fig. 28: Langmuir adsorption isotherms for coating on mild steel in demineralized water

at the mild steel and water boundary. As a result, the intermediates are formed with great difficulty [26-28]. In both, graphs, the linear curve shapes, and R^2 are nearly equal to one, which highlights the good dependence of ln(CR) or ln(CR/T) on thermostat temperature[24]. The higher activation energy value in the presence of Acrylic+8% $Zn_3(PO_4)_2$+5mM AgNPs indicates the higher coating efficiency of the coating.

The plus sign ΔH_a value implies that mild steel oxidation and oxygen absorption happen with the absorption of heat, and these reactions become difficult due to shielding action by acrylic coating [22, 23].

The large negative values of ΔS_a imply that during the formation of an activated complex involved in the slowest steps of mild steel oxidation and oxygen absorption, the regularities on the surface of mild steel are improved [22, 24].

The adsorption concepts

The mechanism involved in adsorption between the molecules of acrylic polymer, with 8% $Zn_3(PO_4)_2$ and 5mM AgNPs and mild steel can be followed by using adsorption isotherm. It is done by applying the fraction of active centers present on the metal surface shielded by molecules of acrylic polymer (θ) to different adsorption isotherms [25]. The most suitable isotherm to explain the shield formation by acrylic polymer on a mild steel surface is well well-known Langmuir adsorption isotherm which is given in Equation (17).

$$\frac{\theta}{1-\theta} = K_{ads.}C \qquad (17)$$

K_{ads} is the adsorption constant when the system attains equilibrium. By taking C_{inh}/θ on the Y-axis and C_{inh} on the X-axis, straight-line plots are obtained with intercept = $\frac{1}{K}$ and are shown in Figs. 27 and 28.

K values were found to be significant, which indicates that acrylic molecules, acrylic molecules with 8% $Zn_3(PO_4)_2$ and 5mM AgNPs which are giving the filler effect, are held on the mild steel surface by the firm force of attraction.

The average linear regression coefficient (R^2) value for the Langmuir graph was 0.99, which further confirms the good correlation between $C_{coating}/\theta$ and $C_{coating}$ and the close-fitting of adsorption of the Acrylic Polymer with 8% $Zn_3(PO_4)_2$ and 5MM AgNPs coating to Langmuir adsorption isotherm.

The average slope of straight lines was nearly equal to one for the coatings. It proves that adsorbed molecules of Coatings do not interact with surrounding molecules and form a monolayer on the mild steel surface.

The dependence of K to the standard free energy of adsorption ($\Delta G°_{ads.}$) is given by (18).

$$K = \frac{1}{C_{water}} e^{\frac{\Delta G^{\circ}_{ads.}}{RT}} \qquad (18)$$

Where C_{water}=55.5 mol/L is the molar concentration of water.

The obtained $\Delta G°_{ads.}$ Values by using Equation (15) are listed in Tables 8 and 9. The negative $\Delta G°_{ads.}$ Values imply that acrylic molecules and acrylic with 8% $Zn_3(PO_4)_2$ and 5mM AgNPs are adsorbed without any external stimuli and are highly inactive on the mild steel surface.

$\Delta H°_{ads}$ and $\Delta S°_{ads}$ were calculated from the thermodynamic Equation (19).

$$\Delta G^{\circ}_{ads} = \Delta H^{\circ}_{ads} - T\Delta S^{\circ}_{ads} \qquad (19)$$

The graph obtained by taking $\Delta G°_{ads}$ on the Y-axis and T on the X-axis gives a straight line with slope = ΔS°_{ads} and intercept = ΔH°_{ads} and are shown in Figs. 29 and 30 for different

Table 8: Thermodynamic parameters for adsorption of coatings on mild steel in a freshwater medium.

Temp. (K)	ΔG ° ads. (kJ/mol)	ΔH ° ads. (kJ/mol)	ΔS ° ads. (kJ/mol.K)
303	-7.36882	-4.046	-0.0109
313	-7.45137		
323	-7.58752		

Table 9: Thermodynamic parameters for adsorption of coatings on mild steel in demineralized water medium.

Temp. (K)	ΔG ° ads. (kJ/mol)	ΔH ° ads. (kJ/mol)	ΔS ° ads. (kJ/mol.K)
303	-7.37852	-3.898	-0.0114
313	-7.46107		
323	-7.59252		

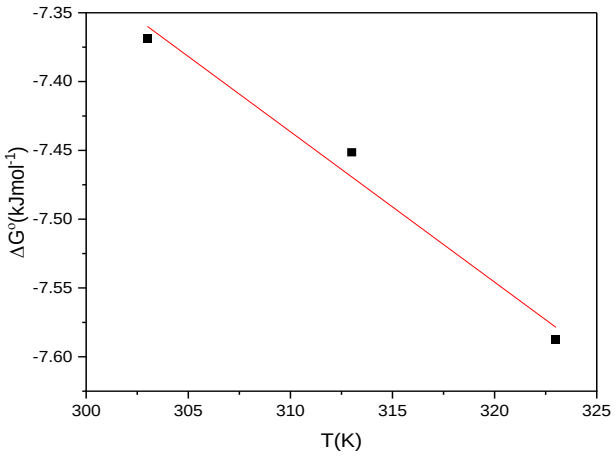

Fig. 29: Plots of ΔG°ads vs. T for adsorption of coatings on mild steel in freshwater

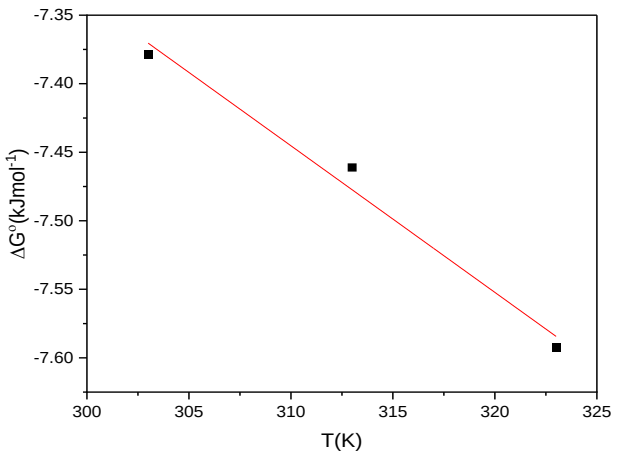

Fig. 30: Plots of ΔG°ads vs. T for adsorption of coatings on mild steel in demineralized water.

coatings for mild steel in fresh and demineralized water. For $\Delta G°_{ads}$ versus T plot, R^2 values are nearly equal to one and the curves are linear, clearly showing the dependence of $\Delta G°_{ads}$ on T and all the energy factors are related to each other. $\Delta H°_{ads}$ and $\Delta S°_{ads}$ values are tabulated in Table 7.

Thermodynamic parameters for adsorption of coatings on mild steel in fresh water and demineralized water medium are shown in Tables 8 & 9.

$\Delta G°_{ads}$ values for acrylic coating with and without 8% $Zn_3(PO_4)_2$ and 5mM AgNPs on mild steel surface were less than –20 kJ/mol. It suggests that the adsorption of polymer on the surface of mild steel is by a weak secondary force of attraction, i.e., the physisorption process [25, 26]. As it contains the polar ester group, or nonpolar group develops the secondary force of attraction with mild steel. The durability of the acrylic coating on mild steel is increased by adding 8% $Zn_3(PO_4)_2$ and 5mM AgNPs, but it will not increase the adsorption tendency of acrylic coating as there is no change in the value of $\Delta G°_{ads}$. From the literature study, it is revealed that the polymer molecules form a secondary force of attraction with the metal surface.

$\Delta H°_{ads.}$ values for acrylic coating on mild steel in freshwater were −4.086 kJ/mol and -3.898 kJ/mol respectively [27]. It implies that the adsorption of the acrylic coating takes place by the physical adsorption as it is a polymer. The $\Delta S°_{ads.}$ value was negative for acrylic adsorption. It confirms the improvement in regularity by adsorption of acrylic molecules on the mild steel surface.

Characterisation

FT-IR spectroscopy

The spectral results are shown at 3505 and 2968 cm^{-1} values assigned to –OH and -CH stretching respectively. The other peak at 1648 cm^{-1} is due to the amide group and 3178 cm^{-1} was assigned to the C–N stretching vibration of the amine group. The FT-IR spectra results formerly reported indicated that the leaves extract phytocompounds [29] such as phytosterol, flavonoids, alkaloids, triterpenoids, amino acids, and proteins might be participating in the process of nanoparticle synthesis.

UV-Spectroscopy

The formation of AgNPs was confirmed using the optical properties analyzed through a UV-Visible spectrophotometer. The maximum absorbance obtained at 430 nm shows the presence of silver nanoparticles. That confirms the reduction of silver ions [29] of silver nitrate to metallic silver by the leaf extract [30-33].

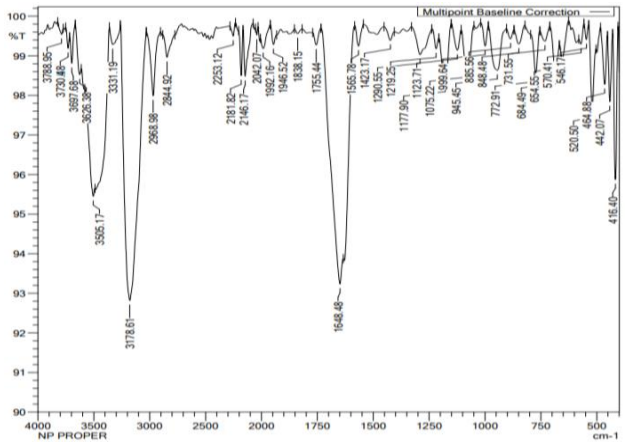

Fig. 31: FT-IR spectra of leaf extract AgNPs

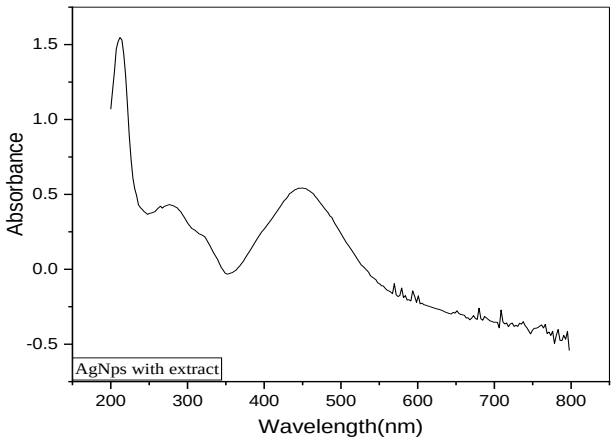

Fig. 32: UV spectra for the presence of AgNPs

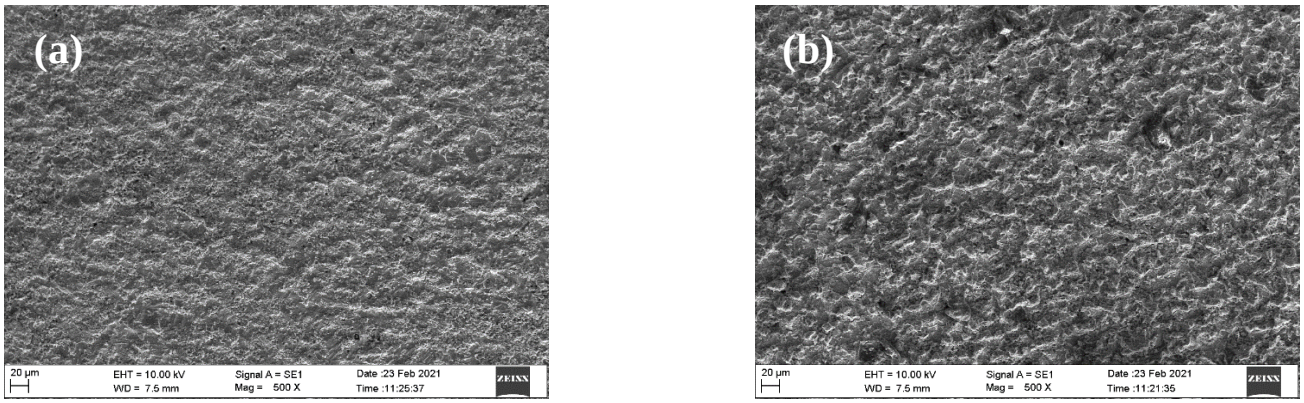

Fig. 33: SEM images of mild steel in (a) Demineralized water and (b) Freshwater

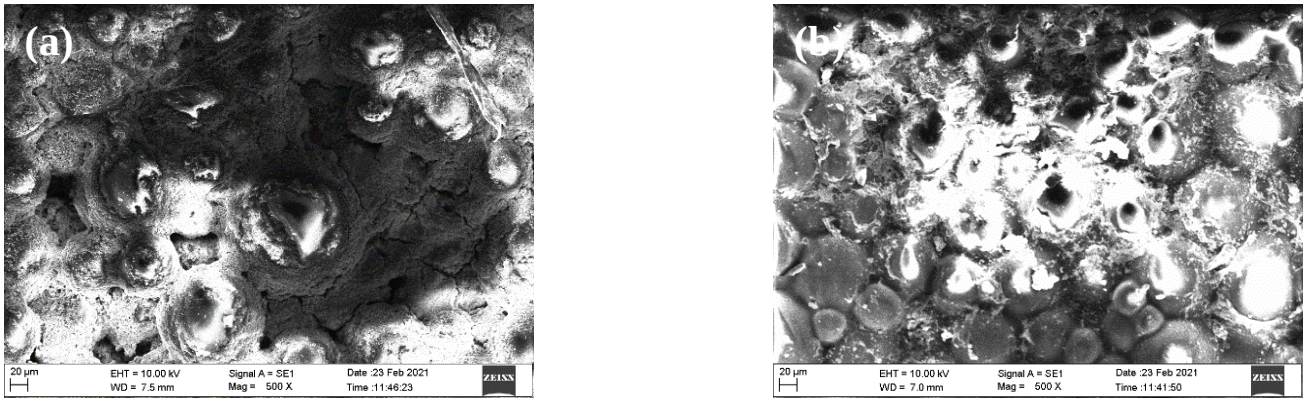

Fig. 34: SEM images of mild steel with acrylic coating in (a) demineralized water and (b) freshwater

Surface Morphology

The SEM images obtained by keeping the mild steel in demineralized, fresh water for three days are given in Fig. 33 (a) and (b).

The SEM image of mild steel in freshwater showed more irregularities compared to demineralized water, which implies that the rate of mild steel dissolution is high in freshwater as it contains many charged ions. The roughness increased with an increase in the number of days of exposure to mild steel.

The SEM images obtained by keeping the mild steel with acrylic coating in demineralized, freshwater for three days is given in Fig. 34 (a) and (b). The images showed the polymer acrylic coating on the mild steel surface.

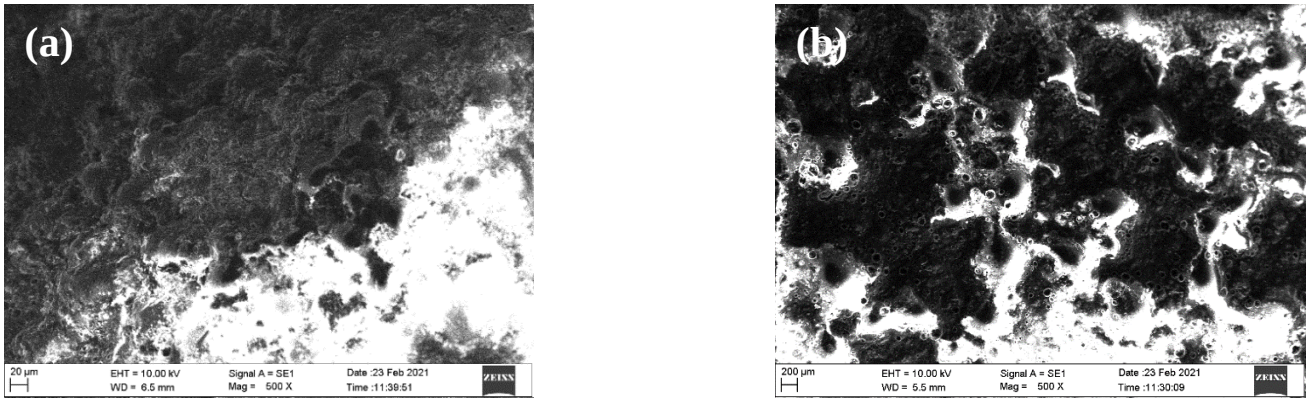

Fig.35: SEM images of mild steel with acrylic+ 8%$Zn_3(PO_4)$ coating in (a) demineralized water (b) freshwater

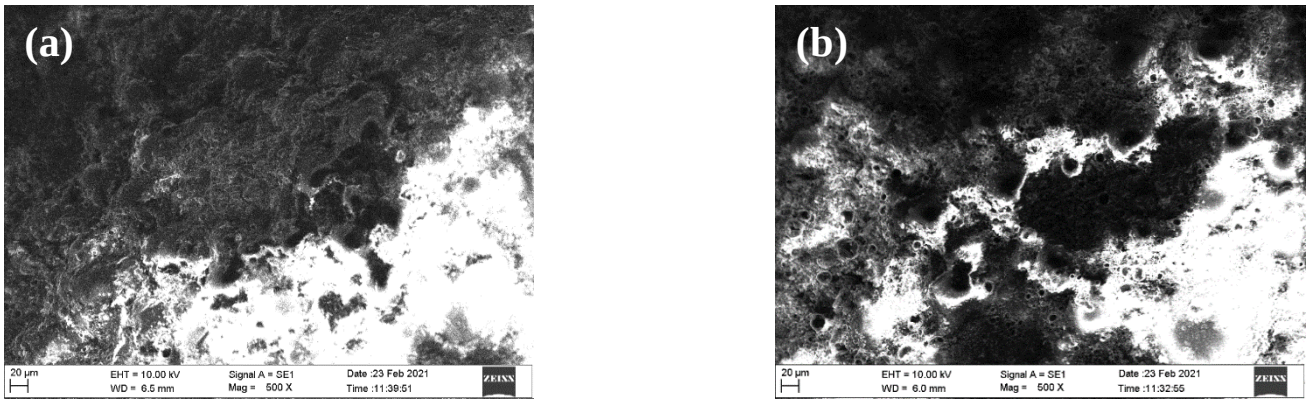

Fig. 36: SEM images of mild steel with Acrylic+ 8% $Zn_3(PO_4)$ +5mM AgNPs coating in (a) demineralized water (b) fresh water

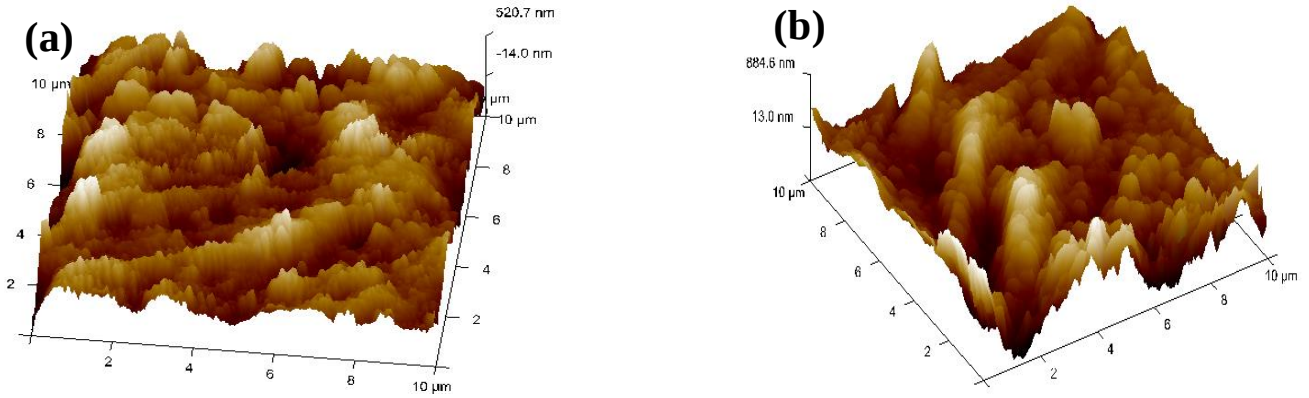

Fig. 37: 3D-AFM images of mild steel in a) Freshwater and b) Demineralised water

The SEM images obtained by keeping the mild steel with acrylic+ 8%$Zn_3(PO_4)$ coating in demineralized, fresh water for three days are given in Fig. 35 (a) and (b). The images showed an increase in the uniformity of the coating, which confirms the reduction in the water absorption nature of the acrylic coating by zinc phosphate.

The SEM images obtained by keeping the mild steel with Acrylic + 8% $Zn_3(PO_4)_2$ + 5mM AgNPs coating in demineralized, fresh water for three days are given in Fig. 36 (a) and (b). The images showed a further increase in the uniformity of the coating, confirming the reduction in the water absorption nature of the acrylic coating by $Zn_3(PO_4)_2$ and AgNPs.

The 3D-AFM images of mild steel kept in fresh water and demineralized water for three days are given in Fig. 37 (a) and (b).

Table 9. Results of AFM analysis

Medium	R_a (nm)	R_q (nm)
Mild steel in demineralized water	146	185
Mild steel in tap water	164	217

The average surface roughness (R_a) and the root mean square roughness (R_q) are given in Table 10. R_a and R_q values are increased as there will be a change of exposure of mild steel from demineralized to tap water. As the corrosivity increases from demineralized to tap water the rate of mild steel oxidation and oxygen absorption reactions on the surface of mild steel. It confirms on the surface of mild steel the extent of roughness increases from demineralized to tap water.

The acrylic coating with and without 8% zinc phosphate on mild steel is hard and hence proper AFM images could not be obtained.

Mechanism of corrosion

Mechanism of corrosion on mild steel.

There are two mechanisms (I) and (II) proposed [34] for the electrochemical reaction of iron corrosion. In both mechanisms, there are two steps in mild steel oxidation, and one of the steps takes place slowly (r.d.s.).

In aqueous solutions: Mechanism (I)

$$Fe + H_2O \rightleftharpoons [FeOH]_{ads} + H^+ + e- \quad (20)$$

$$[FeOH]_{ads} \rightleftharpoons [FeOH]^+_{ads} + e^- \text{ (r.d.s)} \quad (21)$$

$$[FeOH]^+_{ads} + H^+ \rightleftharpoons Fe^{2+} + H_2O \quad (22)$$

In aqueous solutions containing Cl -: Mechanism (II)

$$Fe + H_2O + Cl^- \rightleftharpoons [FeClOH]^-_{ads} + H+ + e^- \quad (23)$$

$$[FeClOH]^-_{ads} \rightleftharpoons [FeClOH]ads + e- \text{ (r.d.s.)} \quad (24)$$

$$[FeClOH]^-_{ads} + H^+ \rightleftharpoons Fe^{2+} + Cl^- + H_2O \quad (25)$$

Cathodic reaction

$$O_2 + 2H_2O + 2e^- \rightleftharpoons OH^- \quad (26)$$

The activated species $[FeOH]_{ads}$ and $[FeClOH]^-_{ads}$ formed in the rate-determining step of mechanisms (I) and (II) are mainly responsible for the oxidation of mild steel. From mechanism (II), it was evident that in the presence of Cl^- in the surrounding iron oxidation occurs through the $[FeClOH]^-_{ads}$ intermediate and through the $[FeOH]_{ads}$ intermediate. But both mechanisms can take place at the same time. Hence, the mild steel surface acquires a positive charge at the anode. This is supported by pourbiax diagrams and the zero-charge potential of mild steel. Therefore, it will stimulate the attack of counter ion Cl^- from the aqueous medium towards itself, and the double layer of opposite ions is formed at the mild steel and H_2O boundary.

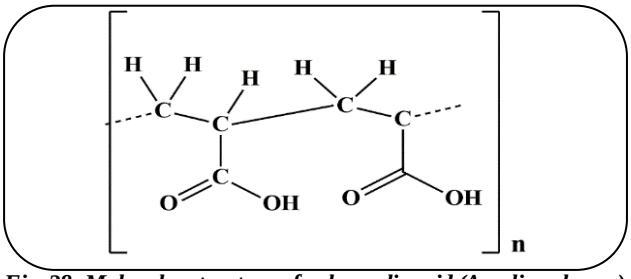

Fig. 38: Molecular structure of polyacrylic acid (Acrylic polymer)

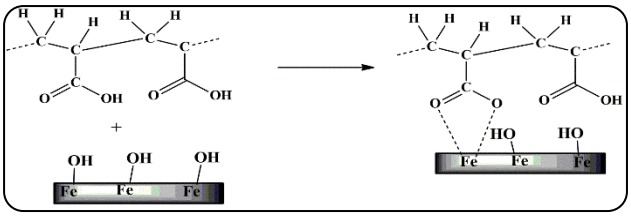

Fig. 39: Adsorption mechanism of acrylic polymer onto the steel surface

Mechanism of corrosion protection

The metal surface has adsorbed OH^-, due to the oxygen absorption. The acrylic coating is a waterborne polymer, and the acid group of acrylic polymers will be present as COO^- which is resonance stabilized. The COO^- group is now adsorbed on the surface by replacing the adsorbed OH^- ion. Hence acrylic coating forms a barrier between the metal and the environment.

On continuously exposing this water-borne polymer to water, the corrosion of mild steel increases as it is permeable to water. The water permeability of the polymer increases the disbonding nature of the acrylic coating. The pigment zinc phosphate is added to increase the shielding power and to decrease the disbonding nature and wet adhesion nature of the acrylic coating. The reason for this may be that, when the corrosive medium penetrates through the waterborne acrylic coating/metal interface, the filler $Zn_3(PO_4)_2$ partly dissolves, and forms metal substrate phosphate and a stabilized protective film, which contains γ-Fe_2O_3, α-FeOOH, γ-FeOOH, and iron phosphate. The formed protective film contains COO^- and -OH groups [32] that improve the interaction of the coating and metal, thereby restricting the diffusion of the medium [35] into the channels and slowing down corrosion.

$$Fe \rightarrow Fe^{2+} + 2e^- \quad (27)$$

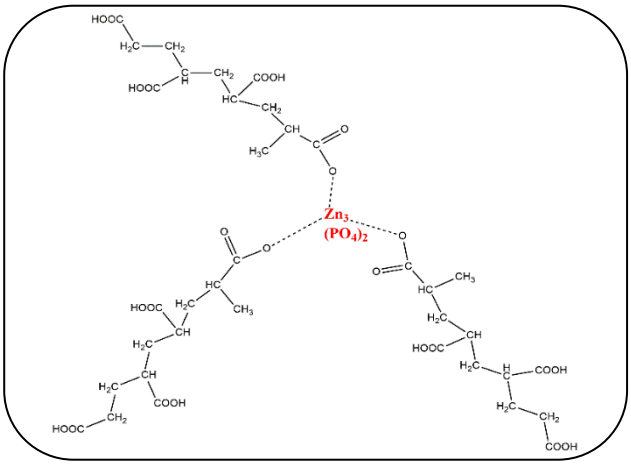

Fig.40: Complex of Acrylic polymer bonded to $Zn_3(PO_4)_2$

$$O_2 + 2H_2O + 4e^- \rightarrow 4OH^- \quad (28)$$

$$Zn_3(PO_4)_2 + 2H_2O + 4OH^- \rightarrow 3Zn(OH)_2 + 2HPO_4^{2-} \quad (29)$$

$$Fe^{2+} + HPO_4^{2-} \rightarrow FePO_4 + H^+ + e^- \quad (30)$$

Zinc phosphate can block the water medium diffusion [35-36]. The corrosion current density in the presence of acrylic with 8% $Zn_3(PO_4)_2$ coating decreased, as the dipping time increased because the chemical activation of zinc phosphate enhanced the wet coating adhesion, the diffusion of the water medium in the coating/metal interface was not permitted, thereby slowing the acrylic coating defect, mild steel oxidation, and oxygen reduction, and disbonding nature of the acrylic coating.

When the acrylic coating with the defect was exposed to a cooling water medium, the mild steel oxidation and oxygen absorption reactions occurred rapidly on the coating/metal interface. Furthermore, the acrylic coating disbonding from the defect. However, the coating defect with $Zn_3(PO_4)_2$ has two features of protection. First, when the cooling water medium permeates the coating/metal interfaces, the $Zn_3(PO_4)_2$ and Fe react and form stable iron phosphates and prohibit mild steel oxidation. Second, $Zn_3(PO_4)_2$ can combine with the carboxyl and hydroxyl groups of the acrylic coating, through which a highly stable and strong protective film is formed by the $Zn_3(PO_4)_2$, acrylic coating, and mild steel substrate. All these reactions can inhibit the oxygen reduction reaction from damaging the acrylic coating, thereby slowing down the acrylic coating defect, mild steel oxidation and oxygen reduction of reactions, and disbonding the nature of the acrylic coating.

The disbonding effect and medium permeability were further reduced by adding the silver nanoparticles to the acrylic coating.

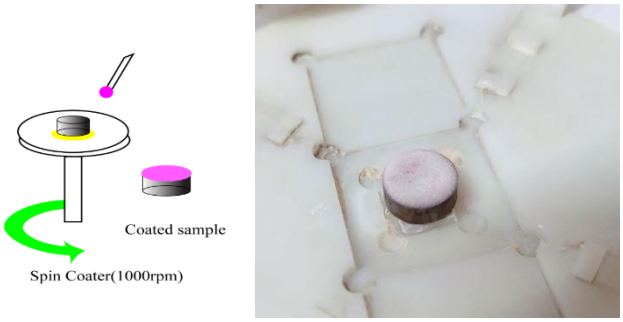

Fig. 41: Spin coating of mild steel

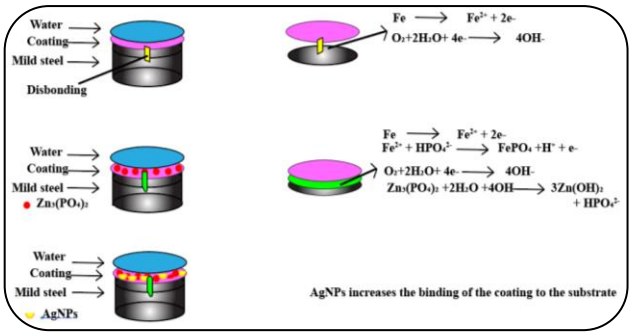

Fig. 42: Mechanism of Corrosion protection

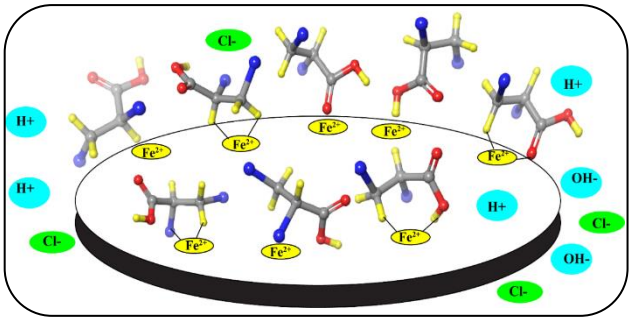

Fig. 43: Different orientations of acrylic molecules during physical adsorption on the mild steel surface

Theoretical studies

The quantum study of acrylic tetramer molecules obtained from the calculations includes E_{HOMO}, E_{LUMO}, $\Delta E = E_{LUMO} - E_{HOMO}$, and dipole moment (μ). Based Frontier Molecular Orbital (FMO), were also calculated, and are listed in Table 10. The optimized structure of acrylic tetramer is shown in Fig. 44 (a) and the optimized geometry of Frontier Molecular Orbitals (FMO) is shown in Fig. 44 (b) and (c).

According to Koopmans's theorem, the E_{HOMO} directly varies with ionization energy (I) [37], as given by Equation (31), which signifies the capacity of the molecule to provide electrons to the vacant orbitals of metals.

$$I = -E_{HOMO} \quad (31)$$

Table 10: Quantum parameters as obtained from the DFT method

ΔE (eV)	E_{HOMO} (eV)	E_{LUMO} (eV)	I (eV)	A (eV)	μ (D)	χ (eV)	η (eV)	ΔN (eV)	ω	S
-0.2681	-0.275	-0.0069	0.275	0.0069	3.423	0.1409	0.134	25.59	43.719	7.459

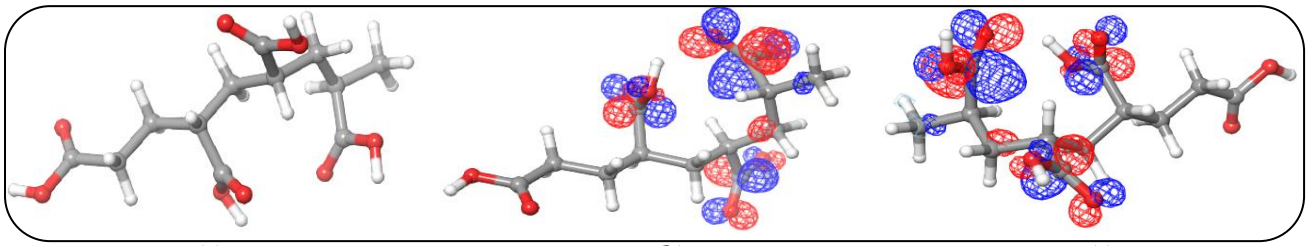

(a) **(b)** **(c)**

Fig. 44: (a) Optimized structure of acrylic tetramer (b) HOMO (c) LUMO of the acrylic tetramer.

The more negative ionization energies of acrylic tetramer [18] indicate high donation ability and high prohibition efficiency.

The E_{LUMO} is the useful reactivity parameter and is directly related to the electron affinity (A) as given in equation (32). Koopmans's theorem also provides this relation.

$$A = -E_{LUMO}. \quad (32)$$

E_{LUMO} signifies the tendency of a molecule to take an electron from a metal. The lower the E_{LUMO}, the stronger the electron-taking capacity of the molecule [38]. Acrylic tetramer has a high value of E_{HOMO} = -0.275eV and a low value of E_{LUMO} = −0.0069 eV. The vacant 3d orbital of mild steel forms a bond with the HOMO of acrylic tetramer and filled 3s and 3p orbital overlap with its LUMO.

According to the FMO theory, the energy gap is related to the coating efficiency of the acrylic tetramer coating. A lower value for the energy gap ($\Delta E = E_{LUMO} - E_{HOMO}$) is known to show good coating efficiency since the energy for electron removal from the last occupied orbital will be less [39]. A good coating material has a greater tendency to provide electrons to the vacant orbital of the metal, and the capability of forming back bonding by accepting electrons from the metal [37, 40-41]. In our study, the energy gap, ΔE= -0.2681.

The HOMO is concentrated mainly on the oxygen atoms (Fig.43 (b)), attributable to the presence of a lone pair of electrons in the oxygen atom of Acrylic polymer. So, the preferred active sites for electron donation in Acrylic are situated in the regions around the oxygen atoms.

The non-uniform distribution of charges on atoms of a molecule gives the dipole moment (μ). A lower value of μ ranging between 3-5 favors the assembly of a coating molecule on the metal surface [41-45] and also signifies the hydrophobic nature of the acrylic molecule. For acrylic μ= 3.423 D, it favors the accumulation of acrylic molecules on the mild steel surface.

The electronegativity (χ) measures the capacity of an atom or group of atoms to take electrons towards itself [39] and was calculated by equation (33).

$$\chi = \frac{I+A}{2} \quad (33)$$

For Acrylic, χ =0.1409 eV which is a low value signifying that acrylic has less electron-attracting tendency.

The global hardness (η) and softness (S) measure the molecule reactivity for adsorption and their stability on the metal surface [46]. The resistance to the transfer of charge by the atom is given by η and calculated.

$$\chi = \frac{I+A}{2} \quad (34)$$

The tendency of an atom or group of atoms to take electrons is given by S and calculated by Equation (35).

$$S = \frac{1}{\eta} = \frac{2}{I-A} \quad (35)$$

For Acrylic, η =0.134 eV and S =7.459 eV. Hardness can be considered as a low value, and softness can be considered as a high value [46-48]. Hence Acrylic can be considered to have good coating properties

ΔN represents the fraction of electrons transferred from the coating molecule to the metallic surface and calculated by equation (36).

$$\Delta N = \frac{\chi_{Fe} - \chi_{inh.}}{2(\eta_{Fe} - \eta_{inh.})} \quad (36)$$

Where (χ_{Fe}, η_{Fe}) and ($\chi_{inh.}$, η_{inh}) represent, χ and η of the metal and the coating molecule and Φ_{Fe} is the work function. For Iron, the theoretical values of χ_{Fe} = 7.0 eV [41] and η_{Fe} = 0 eV [42, 43] have been used. The higher value

the of ΔN, the greater the tendency of the molecule to donate electrons to the metal. In the present study, ΔN = 25.5 eV, the + sign indicates that the coating molecule donates electrons to the metal. ΔN < 3.6 indicates the high coating efficiency of the acrylic molecule.

The global electrophilicity index (ω) is a measure of variation in energy due to the movement of electrons from the donor to the acceptor and is given by *Parr et al*.[39]. It signifies the stabilization in energy produced when the fraction of charge is exchanged between the coating molecule and metal surface [44] and is given by equation (37).

$$\omega = \frac{\mu_P^2}{2\eta} \quad (37)$$

A high value of ω describes a good electrophile, and a small value of ω indicates a good nucleophile. The present study ω = 43.716 eV shows that Acrylic has an excellent capacity to accept electrons from the metal. The coating capacity of acrylic molecules is enhanced by reinforced zinc phosphate and silver nanoparticles.

CONCLUSIONS

- Efficiency of coatings in both fresh and demineralized water was increased with an increase in the addition of fillers and a decrease in temperature from 303 to 323 K.
- Among the 3 coatings, Acrylic+8% $Zn_3(PO_4)_2$ + 5mM AgNPs showed the highest coating efficiency and good corrosion protection for mild steel in fresh and demineralized water.
- The coatings get adsorbed onto the mild steel surface by Physisorption. The rate of corrosion is less in demineralized water and the efficiency of the coating is more in demineralized water.

Received: Jun. 11, 2023; Accepted: Sep. 11, 2023

References

[1] Owolabi H.A., Omidiji B.V., Olugbade E.O., An Investigative Study of Corrosion Effects of Cereals on the Grinding Components of Commercially Available Grinding Machines, *AU Journal of Technology*, **18(1):** 19-26 (2014).

[2] Geethamani P., Kasthuri P.K., Adsorption and Corrosion Inhibition of Mild Steel in Acidic Media by an Expired Pharmaceutical Drug, *Cogent chemistry*, **1(1):** 1091558 (2015).

[3] Herro H.M., Port R.D., "Cooling Water System Design and Operation. The Nalco Guide to Cooling Water System Failure Analysis", 1-12 (1993).

[4] Hojatollah J., Iman D., Hadi E., Electrochemical and Theoretical Studies of Adsorption and Corrosion Inhibition of NN'-Bis(2-Hydroxyethoxyacetophenone) -2,2-Dimethyl-1,2-Propanediimine on Low Carbon Steel(API 5L Grade B)in Acidic Solution, *Ind. Eng. Chem. Res*., **52(20):** 6617–6632 (2013).

[5] Hamedraza J., Mousa G., Mehdi T., Adsorption Kinetics,isotherm, and Thermodynamics of Hg^{2+} to Polyaniline/Hexagonal Mesoporous Silica Nanocomposite in Water/Wastewater, *J. Mater. Sci.*, **49:** 232–242 (2014).

[6] Hojat J., Kazem A., Iman D., Corrosion Inhibition Of Carbon Steel Immersed in A 1M Hcl Solution Using Benzothiazole Derivatives, *Arabian Journal of Chemistry*, **12(7):** 1387-1394 (2019).

[7] Ramezanzadeh B., Raeisi E., Mahdavian M., Studying Various Mixtures of 3-Aminopropyltriethoxysilane (APS) and Tetraethylorthosilicate (TEOS) Silanes on the Corrosion Resistance of Mild Steel and Adhesion Properties of Epoxy Coating, *International Journal of Adhesion and Adhesives*, **63:** 166-176 (2015).

[8] González-García Y., González S., Souto R.M., Electrochemical and Structural Properties of a Polyurethane Coating on Steel Substrates for Corrosion Protection, *Corrosion Science*, **49(9):** 3514-3526 (2007).

[9] Liu B., Zhang X., Xiao G.Y., Lu Y.P., Phosphate Chemical Conversion Coatings on Metallic Substrates for Biomedical Application: A Review, *Mat. Sci. Eng.: C*, **47:** 97-104 (2015).

[10] Arthanareeswari M., Kamaraj P., Tamilselvi M., Devikala S., A Low Temperature Nano TiO2 Incorporated Nano Zinc Phosphate Coating on Mild Steel with Enhanced Corrosion Resistance, *Materials Today: Proceedings*, **5(2):** 9012-9025 (2018).

[11] Zhou Y., Xiong J., Yan F., The Preparation and Characterization of a Nano-CeO_2/Phosphate Composite Coating on Magnesium Alloy AZ91D, *Sur. Coat. Tech.*, **32:** 335-343 (2017).

[12] Fouladi M., Amadeh A., Comparative Study between Novel Magnesium Phosphate and Traditional Zinc Phosphate Coatings, *Materials Letters*, **98:** 1-4 (2013).

[13] Tamilselvi M., Kamaraj P., Arthanareeswari M., Devikala S., Nano Zinc Phosphate Coatings for Enhanced Corrosion Resistance of Mild Steel, *Applied Surface Science*, **327:** 218-225 (2015).

[14] Osama A., Ahmed A.N., Ionic Liquid-Assisted Production of Hydrophobic Nanocomposite Coating for Mild Steel Corrosion Prevention in Saline Medium, *Journal of Materialsresearch and Technology*, **18:** 5087-5102 (2022).

[15] Mobina M., Milad R., Construction of Highly Anti-Corrosion and Super-Hydrophobic Polypropylene/ Graphene Oxide Nanocomposite Coatings on Carbon Steel .Experimental,Electrochemical and Molecular Dynamics Studiies., construction and building materials, **317:** 125136-125151 (2022).

[16] Sheng M., Wang Y., Zhong Q., Wu H., Zhou Q., Lin H., The Effects of Nano-SiO_2 Additive on the Zinc Phosphating of Carbon Steel, *Surface and Coatings Technology*, **205(11):** 3455-3460 (2011).

[17] Shibli S.M.A., Chacko F., Development of Nano TiO_2-Incorporated Phosphate Coatings on Hot Dip Zinc Surface for Good Paintability and Corrosion Resistance, *Applied Surface Science*, **257(7):** 3111-3117 (2011).

[18] Dastmalchian H., Moradian S., Jalili M.M., Mirabedini S.M., Investigating Changes in Electrochemical Properties When Nano-Silica Is Incorporated into an Acrylic-Based Polyurethane Clearcoat, *Journal of Coatings Technology and Research*, **9(2):** 195-201 (2012).

[19] Eduok U., Szpunar J., Ebenso E., Synthesis and Characterization of Anticorrosion Zirconia/Acrylic Nanocomposite Resin Coatings for Steel, *Progress in Organic Coatings*, **137:** 105337 (2019).

[20] Lerga T.M., O'Sullivan C.K., Rapid Determination of Total Hardness in Water using Fluorescent Molecular Aptamer Beacon, *Analytica Chimica Acta*, **610(1):** 105-111 (2008).

[21] Li W.H., He Q., Pei C.L., Hou B.R., Experimental and Theoretical Investigation of the Adsorption Behavior of New Triazole Derivatives as Inhibitors for Mild Steel Corrosion Inacidmedia, *Electrochim. Acta*, **52:** 6386-6397 (2007).

[22] Mansfeld F., Lin S., Kim S., Shih H., Electrochemical Impedance Spectroscopy as a Monitoring Tool for Passivation and Localized Corrosion of Aluminum Alloys, *Mater. Corros.*, **39(11):** 487-492 (1988).

[23] Mansfeld F., Lin S., Kim K., Shih H., Pitting and Surface Modification of SIC/Al, *Corrosion Science*, **27(9):** 997-1000 (1987).

[24] Bessone J.B., Salinas D.R., Mayer C.E., Ebert M., Lorenz W.J., An EIS Study of Aluminium Barrier-Type Oxide Films Formed in Different Media, Electrochimica Acta, 37(12): 2283-2290 (1992).

[25] Shen C.B., Wang S.G., Yang H.Y., Long K., Wang, F.H., Corrosion Effect of Allylthiourea on Bulk Nanocrystalline Ingot Iron in Diluted Acidic Sulphate Solution, *Electrochimica acta*, **52(12):** 3950-3957 (2007).

[26] Wei-Hua L., Qiao H., Sheng-Tao Z., Chang-Ling P., et al., Some New Triazole Derivatives as Inhibitors for Mild Steel Corrosion in Acid Medium, *J. Appl. Electrochem.*, **38(3):** 289-295 (2008).

[27] Machnikova E., Kenton W.H., hackerman N., Corrosion Inhibition of Carbon Steel in Hydrochloric Acid by Furan Deravatives, *Electrochim. Acta*, **53:** 6024-6032 (2008).

[28] Singh A.K., Quraishi M.A., Effect of Cefazolin on the Corrosion of Mild Steel in HCl Solution, *Corros. Sci.*, **52:** 152-160 (2010).

[29] Seoudi R., El-Bahy G.S., El Sayed Z.A., FT-IR, TGA and DC Electrical Conductivity Studies of Phthalocyanine and its Complexes, *Journal of Molecular Structure*, **753(1-3):** 119-126 (2005).

[30] Bayo K., Mossoyan J.C., Ouedraogo G.V., Preparation and Analysis by UV-Vis of Zinc Phthalocyanine Complexes, *Spectrochimica Acta Part A: Molecular and Biomolecular Spectroscopy*, **60(3):** 653-657 (2004).

[31] Sathyavathi R., Krishna M.B., Rao S.V., Saritha R., Rao D.N., Biosynthesis of Silver Nanoparticles using Coriandrum Sativum Leaf Extract and their Application in Nonlinear Optics, *Advanced Science Letters*, **3(2):** 138-143 (2010).

[32] Vinay S.P., Chandrasekhar N.U., Ixora Coccinea Extract-Mediated Green Synthesis of Silver Nanoparticles: Photodegradative and Antimicrobial Studies, *Int. J. Biosen. Bioele.*, **5(4):** 100-105 (2019).

[33] Karuppiah M., Rajmohan R., Green Synthesis of Silver Nanoparticles Using Ixora Coccinea Leaves Extract, *Materials Letters*, **97:** 141-143 (2013).

[34] El-Awady A.A., Abd-El-Nabey B.A., Aziz S.G., Thermodynamic and Kinetic Factors in Chloride Ion Pitting and Nitrogen Donor Ligand Inhibition of Aluminium Metal Corrosion in Aggressive Acid Media, *Journal of the Chemical Society, Faraday Transactions*, **89(5):** 795-802 (1983).

[35] Romagnoli R., Vetere V.F., Heterogeneous Reaction between Steel and Zinc Phosphate, *Corrosion*, **51(2):** 116-123 (1995).

[36] Caprari J.J., Di Sarli A.R., Del Amo B., Zinc Phosphate as Corrosion Inhibitive Pigment of Waterborne Epoxy Paints Used for Steel Protection, *Pigment & resin technology*, **38:** 289-295 (2000).

[37] Adejoro I.A., Akintayo D.C., Ibeji C.U., The Efficiency of Chloroquine as Corrosion Inhibitor for Aluminium in 1M HCl Solution: Experimental and DFT Study, *Jordan Journal of Chemistry*, **11(1):** 38-49 (2016).

[38] Musa A.Y., Kadhum A.A.H., Mohamad A.B., Rahoma A.A.B., Mesmari H., Electrochemical and Quantum Chemical Calculations on 4, 4-Dimethyloxazolidine-2-Thione as Inhibitor for Mild Steel Corrosion in Hydrochloric Acid, *Journal of Molecular Structure*, **969(1-3):** 233-237 (2010).

[39] Ashassi-Sorkhabi H., Shaabani B., Seifzadeh D., Corrosion Inhibition of Mild Steel by some Schiff base Compounds in Hydrochloric Acid, *Applied Surface Science*, **239(2):** 154-164 (2005).

[40] Arukalam I.O., Durability and Synergistic Effects of KI on the Acid Corrosion Inhibition of Mild Steel by Hydroxypropyl Methylcellulose, *Carbohydrate polymers*, **112:** 291-299 (2014).

[41] Koopmans T., About the Assignment of Wave Functions and Eigenvalues to the Individual Electrons of an Atom, *Physica.*, **1(1-6):** 104-113 (1934).

[42] Parr R.G., Pearson R.G., Absolute Hardness: Companion Parameter to Absolute Electronegativity, *Journal of the American Chemical Society*, **105(26):** 7512-7516 (1983).

[43] Pearson R.G., Hard and Soft Acids and bases—the Evolution of a Chemical Concept, *Coordination Chemistry Reviews*, **100:** 403-425 (1980).

[44] Sastri V.S., Perumareddi J.R., Molecular Orbital Theoretical Studies of some Organic Corrosion Inhibitors, *Corrosion*, **53(08):** NACE-97080617 (1997).

[45] Martinez S., Inhibitory Mechanism of Mimosa Tannin Using Molecular Modeling and Substitutional Adsorption Isotherms, *Materials Chemistry and Physics*, **77(1):** 97-102 (2003).

[46] Dewar M.J., Thiel W., Ground States of Molecules. 38. The MNDO Method. Approximations and Parameters, *Journal of the American Chemical Society*, **99(15):** 4899-4907 (1977).

[47] Yan Y., Li W., Cai L., Hou B., Electrochemical and Quantum Chemical Study of Purines as Corrosion Inhibitors for Mild Steel in 1 M HCl Solution, *Electrochimica Acta*, **53(20):** 5953-596 (2008).

[48] Khosroshahi E.S., Edijali L., Behmagham F., Bahazadeh M.,Ghasemi F., A Density Functional theory study on possible Sensing of Boron Nitride Nanosheet and Its Doped Deravative over the Amantadine Drug, *Iranian Journal of Chemistry and Chemical Engineering (IJCCE)*, **41(7):** 2213-2221 (2022).